UNIVERSITY OF CALIFORNIA

Santa Barbara

Sensory inputs to *Drosophila* sequential grooming

A dissertation submitted in partial satisfaction of the

requirements for the degree Doctor of Philosophy

in Molecular, Cellular and Developmental Biology

by

Neil Zhang

Committee in charge:

Professor Julie H. Simpson, Chair

Professor Kenneth S. Kosik

Professor Matthieu Louis

Professor Craig Montell

March 2021

The dissertation of Neil Zhang is approved.

_____
Kenneth S. Kosik

_____
Matthieu Louis

_____
Craig Montell

_____
Julie H. Simpson, Committee Chair

March 2021

Sensory inputs to *Drosophila* sequential grooming

By

Neil Zhang

ACKNOWLEDGEMENTS

First, I want to thank my advisor, Dr. Julie H. Simpson. Julie supported me throughout my Ph.D. study. She gave me guidance to figure out what is the most important question and encouraged me whenever I had problems with my project. I feel grateful for the freedom I get both for my research and for my career development.

Julie also brings together a wonderful group of people in the lab. Li Guo gave me a lot of help for the experiments. Dr. Primoz Ravbar and Joshua M. Mueller assisted me for quantitative data analysis. Dr. Shingo Yoshikawa and Dr. Sunanda Marella provided great supports in both the research and lab management. Dr. Durafshan Sakeena Syed gave me many suggestions during lab meetings. Carla Ladd brought great talents for both science and art to the lab. Finally, I also want to thank all the previous and current undergraduates, including Reid Nakamoto and Natalie Manier.

I also thank my committee members: Dr. Craig Montell, Dr. Matthieu Louis and Dr. Kenneth S. Kosik. Craig always has great passion for science. I still remember his excellent talk in NIBS which I attended in my senior year of undergraduate study. Matthieu provided precious feedbacks for my manuscript, which helped me analyze all the data more rigorously. Ken always encourages me to think outside the box.

I would like to acknowledge other faculty members and staffs in MCDB department. Dr. Joel Rothman and Dr. Bill Smith generously provided us lab space for 3 years. I learned a lot from the discussion with Dr. Sung Soo Kim during our

joint lab meetings. Dr. Kathy Foltz and Anthony Galaviz helped me meet all the requirements from the department. I have also received a lot of support from other graduate student colleagues.

I have been fortunate to meet my friends and roommates during my graduate study. They helped me go through all the challenges I had as an international student.

Finally, I thank my parents for their support. They always encourage me to make my own decisions. They give me great freedom to explore all the possibilities for my life.

Curriculum Vitae: NEIL ZHANG

EDUCATION

Ph.D. Molecular, Cellular & Developmental Biology (2021)
University of California, Santa Barbara (UCSB)
B.S. Biological Sciences (2015)
China Agricultural University

PROFESSIONAL EMPLOYMENT

UCSB MCDB Department, Santa Barbara, CA
Graduate Researcher, Prof. Julie H. Simpson Lab June 2016 – March 2021
Sensory inputs to *Drosophila* sequential grooming
Graduate Teaching Assistant, Genetics Course Winter 2016 – 2019

Pharmacyclics, Sunnyvale, CA
Research Intern, Translational medicine department Jun 2019 – Aug 2019
Using single cell sequencing to investigate the mechanism of action of ibrutinib

PUBLICATIONS

Zhang, N., Guo, L., and Simpson, J.H. (2020). Spatial Comparisons of Mechanosensory Information Govern the Grooming Sequence in *Drosophila*. Curr. Biol. *30*, 988-1001 [1].

CONFERENCE AND PRESENTATIONS

The Protein Science Week 2020

Comparisons of mechanosensory information in space at different time points control *Drosophila* grooming sequence, Poster, CSHL Neurobiology of *Drosophila* conference 2019

Mechanosensory inputs contribute to the sequence of *Drosophila* grooming, Poster, Society for Neuroscience annual meeting 2018

Sensory inputs strength and dynamics contribute to grooming sequence in *Drosophila*, Talk, UCSB Neuroscience Symposium 2018

ABSTRACT

Sensory inputs to *Drosophila* sequential grooming

by

Neil Zhang

Animals integrate information from different sensory modalities, body parts, and time points to inform behavioral choice, but the relevant sensory comparisons and the underlying neural circuits are still largely unknown. I use the grooming behavior of *Drosophila melanogaster* as a model to investigate the sensory comparisons that govern a motor sequence. Flies perform grooming movements spontaneously, but when covered with dust, they clean their bodies following an anterior-to-posterior sequence.

In the first part of this dissertation (chapter 2), I investigated the functions of different sensory modalities in grooming. I found multiple types of mechanosensory neurons can induce *Drosophila* grooming; other sensory modalities are not required. The grooming behaviors induced by different sensory organs are very different. Only activation of bristle neurons distributed over the body results in an anterior-to-posterior grooming sequence, similar to dust-induced grooming.

In the second part of this dissertation (chapter 3), I investigated how sensory inputs contribute to grooming sequence. Computational modeling predicts that higher sensory input strength to the head will cause anterior grooming to occur first.

I tested this prediction using an optogenetic competition assay where two targeted light beams independently activate mechanosensory bristle neurons on different body parts. I found that the initial choice of grooming movement is determined by the ratio of sensory inputs to different body parts. In dust-covered flies, sensory inputs change as a result of successful cleaning movements. Simulations from our model suggest that this change results in sequence progression. One possibility is that flies perform frequent comparisons between anterior and posterior sensory inputs, and the changing ratios drive different behavior choices. Alternatively, flies may track the temporal change in sensory input to a given body part to measure cleaning effectiveness. The first hypothesis is supported by our optogenetic competition experiments: iterative spatial comparisons of sensory inputs between body parts is essential for organizing grooming movements in sequence.

In the last part of this dissertation (chapter 4), I investigated the neural circuit that processes sensory inputs from wing campaniform sensilla. Secondary interneurons are found in both brain and ventral nervous cord. Through an anatomy-guided behavior screen, I identified a group of interneurons which can induce wing grooming ipsilaterally.

TABLE OF CONTENTS

Contents

1. Introduction

To organize a complex behavior, the nervous system needs to integrate sensory information from different types of sensory organs on different body parts. The absolute and relative sensory inputs to these body parts change over time. For example, dust can induce grooming behavior in *Drosophila melanogaster*. When the fly is covered with dust, sensory organs all over the body are activated, but only one part is groomed at a time. The distribution of dust across the body changes as a result of grooming movements, so flies may be constantly re-assessing the relative amounts of dust. Therefore, *Drosophila* grooming provides a good platform to study the rules for integrating diverse time-varying sensory inputs.

Motor actions can be organized into sequences, and animals use sensory feedback to adjust their choice of actions over time. While flies execute some grooming movements spontaneously, the anterior-to-posterior grooming progression is only observed in dust-covered flies. Here, I investigate how sensory stimulation induced by dust may contribute to the organization of grooming sequence. Understanding which groups of sensory neurons are activated by dust will help us dissect this process.

Mechanosensory organs play an essential role in the detection of mechanical irritants [2,3]. The structure and distribution of different mechanoreceptors have been well studied in *Drosophila*, but their contributions to grooming – sensing dust, coordinating legs – remain to be deciphered.

1.1 Mechanoreceptors in adult *Drosophila*

Mechanosensation is essential for insects' sensorimotor control in complex environments. It is fast and robust in both light and dark. Six groups of mechanosensory organs are found in adult flies: bristle, chordotonal organ, campaniform sensilla, hair plate, stretch receptor and multidendritic neuron (Figure 1) [4,5]. They have different structures and respond to different types of mechanosensory inputs. According to the morphology difference, mechanoreceptors can be classified into type I and type II sensory organs [6].

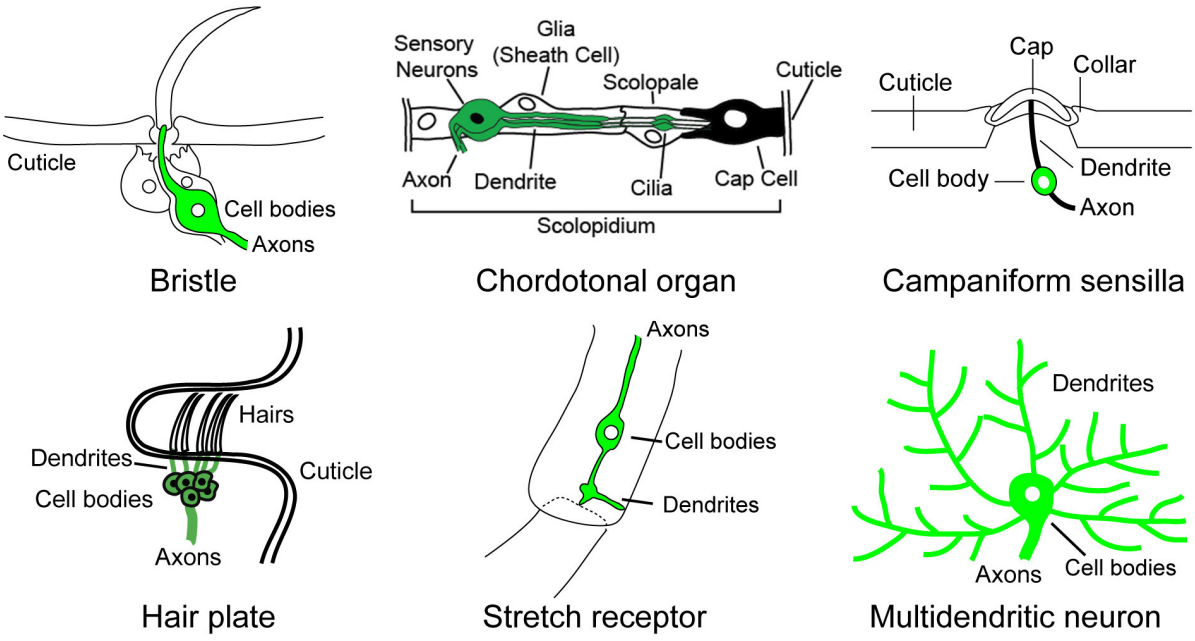

Figure 1. Mechanosensory organs in adult *Drosophila*
Schematic of 6 kinds of mechanosensory organs in adult fruit flies. Bristle, chordotonal organ, campaniform sensilla and hair plate belong to type I organs. Stretch receptor and multidendritic neuron belong to type II organs. Chordotonal organ diagram is taken from Wikimedia Commons (Page Version ID: 378844076) under CC 4.0 license. Campaniform sensilla diagram is taken from Wikimedia Commons (Page Version ID: 361979774) under CC 4.0 license. Hair plate diagram is taken from Wikimedia Commons (Page Version ID: 351478553) under CC 4.0 license. The other diagrams are drawn based on [4,5].

1.1.1 Type I organs

Type I organs include bristle, chordotonal organ, campaniform sensilla and hair plate. They have specialized cuticle structure and are associated with mechanosensory neurons with single dendrite.

Tactile hairs or mechanosensory bristles are the most abundant mechanosensory exteroceptors in adult flies. Their external part is a closed bristle shaft. Each shaft connects to a single neuron through dendritic cap. The shaft functions as a lever to amplify small movements and activates mechanosensory channels located on the dendrites. Extracellular recordings have been made by bristles on the notum and legs [7,8]. Transduction current can be induced by small displacements with a latency around only 0.2ms. The response also shows direction selectivity. Most bristles form a ~45° angle relative to the cuticle. Stronger and more robust response is induced by deflection toward the body. As exteroceptors, bristles alert flies the existence of foreign objects such as other individuals or mites [2,3]. Bristles seem to also provide proprioceptive inputs because mutants lacking bristle function or flies with leg bristle neurons inhibition show decreased limb coordination [5,6].

Chordotonal organs are located between body joints of antennae, legs, wings, halteres and abdomen. The scolopidium is the fundamental unit of chordotonal organs (Figure 1). Each scolopidium contains 1-3 bipolar mechanosensory neurons and two supporting cells: scolopale encloses the dendrites; cap cell connects the dendrite tip to cuticles [4]. Chordotonal organs can function as either exteroceptors or proprioceptors. The Johnston's organ (JO) is the largest group of chordotonal organs. It is located in the second segment of antenna, where it detects relative

movements between the second segment and distal segment induced by sound, wind, gravity or contact deflection [9,10]. Leg chordotonal organs are thought to be the main proprioceptors in the legs. Approximately 135 chordotonal organ neurons are located in the femur. They can be further divided into subgroups that encode tibia position, movement and vibration [11].

Campaniform sensilla are associated with an oval shape cuticular dome. The compression of this specialized cuticle structure activates the mechanosensory neuron underneath. Campaniform sensilla are located on legs, wings and halteres. Halteres are dumbbell-shaped organs which evolved from ancestral hindwings. They beat in antiphase with wings at the same frequency during flight. The 100 campaniform sensilla at the base of each haltere [6] sense Coriolis forces induced by body rotation, thus acting as a gyroscope during flight [12]. Approximately 35 campaniform sensilla are found on each leg. They can be divided into three groups according to the axon projections: the first group projects locally to its own neuromere. The second group projects to ipsilateral neuromeres corresponding to other legs. The third group, bilateral campaniform sensillum (bCS) innervate multiple neuromeres both ipsilaterally and contralaterally. bCS neurons form direct synapses with the same motor neurons on both sides of the body. This symmetrical projection indicates they may function as load sensors to help flies keep stable posture [13].

Hair plates are clustered short tactile hairs. They are found on the leg joints between coxa and thorax as well as between cox and trochanter [8]. They will be deflected during leg movements and provide proprioception inputs for walking.

1.1.2 Type II organs

Two types of type II organs are found in adult flies: stretch receptor and multidendritic neuron. They are neurons with multiple dendritic branches that connect with cuticle directly.

Stretch receptors are found between leg joints. Their two dendrites connect with neighboring leg segments. Calcium imaging shows that the changing joint angle induces dendritic stretch and elicits neural activity [14].

Multidendritic neurons are well studied in larva, different subtypes can function as either exteroceptors or proprioceptors. In adult flies, multidendritic neurons can be found in labellum and abdomen. Multidendritic neurons in the labellum help flies detect food texture [15]. Behavior experiments indicate that multidendritic neurons in the abdomen play a role in blue light avoidance [16].

1.2 Behavior sequence and its control

Motor actions are usually organized into a coordinated sequence. Sequential behaviors can be classified as innate sequential behavior or learned sequential behavior. Innate sequential behaviors are mainly specified genetically during development and can be performed by animals without prior experience. Learned sequential behaviors are developed as a result of experience. Behavioral sequences have been described in multiple species [17–20], but the underlying neural control elements were only investigated in few examples. It is still unclear whether there are shared core mechanisms. I use *Drosophila* grooming behavior to investigate how an innate behavior sequence is controlled by nervous system.

1.2.1 Innate sequential behaviors

During *Drosophila* courtship, males perform sequential motor actions including female orienting, wing singing, licking, tapping and abdomen bending. McKellar et al [21] found that the final stage of courtship is controlled by one pair of descending neurons, aSP22. Optogenetic stimulation of aSP22 induces the same sequence: proboscis extension → abdomen curling → leg lifting. These sequential behaviors can accumulate, flies usually perform all three at the same time in the end. Using *ex-vivo* patch-clamp recordings, they proposed a “ramp-to-threshold” mechanism, suggesting latter behavior is performed once a neural activity threshold is reached. Interestingly, the thresholds are best explained by spike count rather than spike frequency.

Grooming is very important for animals to remove parasites and keep their sensory organs clean. Fruit flies spend 13% of waking time performing spontaneous

grooming behavior [22]. When covered with dust, they follow an anterior-to-posterior sequence to clean their bodies. Flies can only clean one body part at a time. Therefore, different from courtship behavior, grooming motifs are mutually exclusive. This grooming sequence can be explained by our previous model based on parallel activation of different grooming modules with hierarchical suppression between them [23]. In this project, I further test this model by combing optogenetic manipulation with a fly-on-a-ball setup. I also investigate how changing sensory inputs affect the grooming sequence.

1.2.2 Learned sequential behaviors

Many animals including us have extraordinary capacity for learning novel motor skills. Young zebra finches can produce highly variable babbling songs. During development, they hear, memorize and learn the song of an older bird. After approximately 60 days of practice, the song crystallizes into an adult song with sequential structure. The adult song consists of 2-7 motifs. Each motif is composed of a stereotyped sequence of syllables [24]. This vocal sequence is encoded by the neural activity propagation through synaptic connected HVC neurons. Each individual premotor HVC neuron bursts at a single moment in the song [25]. Different neurons form a chain of activity which corresponds to the whole duration of song.

To study how the learned motor sequences are organized in the nervous system in mammals, Geddes et al. [26] designed an operant task in which mice need to learn to press the two levers in a specific sequence “left-left-right-right” (LLRR) to get food reward. They found mice learned RR first, followed by LL subsequence. This suggests that behavior elements are organized into subsequences LL, RR and

then connected into full sequence. They also found stratum NMDA receptors play an essential role in sequence learning. To further investigate how behavioral sequence is encoded in stratum, they first performed electrophysiology recordings in stratum area. Different groups of neurons show stage-specific neural activities: striatal D1- expressing spiny projection neurons (dSPNs) are more active at sequence initiation and termination. Striatal D2- expressing spiny projection neurons (iSPNs) are more active during transition between subsequences. They also tested the roles of different neuron populations by optogenetics. Stimulation of dSPNs delayed sequence initiation without affecting sequence structure. Stimulation of iSPNs abolish left subsequence, the right subsequence remains intact. These results suggest the hierarchical organization of action sequences: subsequences are encoded independently and then concatenated into full sequence. dSPNs promote sequence initiation and termination, while iSPNs encode subsequences transitions.

The ability to learn novel motor sequence helps animals perform more complex behaviors and adapt to changing environments. Learned sequential behaviors can be encoded differently by different neuronal populations: in bird song, sequence is organized in serial through an activation chain; in mice levers pressing, sequence is organized in a hierarchical structure with multiple layers of control. In both cases, training changes the connections between these neural populations, establishing novel sequence through neural plasticity.

1.3. Dust-induced anterior-to-posterior grooming sequence in *Drosophila*

Our previous research showed that dust can induce an anterior-to-posterior grooming sequence in *Drosophila* [23]. I use a newly developed automatic behavior recognition system to analyze grooming in large scale [27]. Anterior and posterior grooming motifs contain different grooming subroutines. In the anterior motif, flies use their front prothoracic legs to clean their heads, then discard dust through front leg rubbing. Posterior grooming motif contains body sweeps with back metathoracic legs and back leg rubbing (Figure 2A). Flies perform grooming, walking and standing in our assay. Grooming was observed in undusted flies and the leg movements are similar, but dust increases the grooming time (Figure 2B).

All dust-covered flies groom their anterior body parts first and then posterior ones, but the sequence is not exclusively unidirectional: flies switch back and forth between anterior and posterior grooming motifs and the behavior records from different individuals show variability (Figure 2C). I developed several ways to quantify grooming progression by aggregating data from many flies. One measures probability of performing anterior or posterior grooming movements or walking at each timepoint. While anterior and posterior grooming probabilities are relatively stable throughout the assay in undusted flies, they vary reciprocally in dusted ones: the probability of anterior grooming starts high and declines, while the probability of posterior grooming starts low and increases over time. A “steady-state” is eventually reached, where the probabilities of anterior and posterior grooming movements are approximately equal, although the probability of performing any grooming movement remains high (Figure 2D). I also quantified the ratio of anterior grooming

to posterior grooming within 150s intervals (abbreviated to A:P grooming ratio, and referring to the behavioral outputs). In dusted flies, the A:P grooming ratio is highest at the beginning and decreases gradually. This trend is not observed in undusted flies, where the A:P grooming ratio is not significantly different among all intervals (Figure 2E).

Since dust can induce a sequence of grooming movements, I focus on two questions here: (1) what kind of sensory inputs are essential for grooming? and (2) how do these sensory inputs contribute to the behavioral sequence?

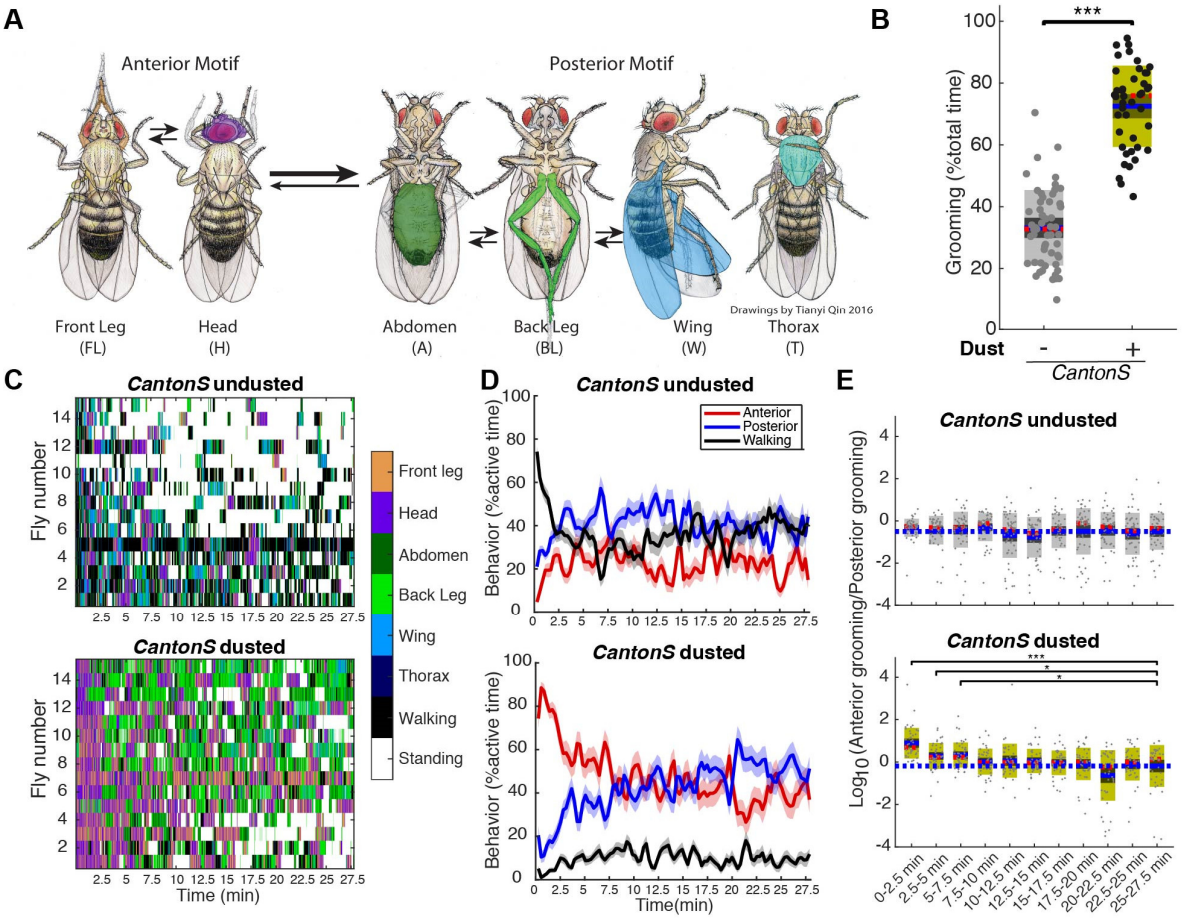

Figure 2. Dust induces anterior-to-posterior grooming sequence in *Drosophila*
(A) Diagram of stereotyped, recognizable grooming movements observed in *Drosophila melangaster*. Arrows indicate most common transitions, and the colored body parts correspond to the movements quantified in subsequent ethograms.

Drawings by Tianyi Qin based on [28]. (B) The percent of time that undusted or dusted flies perform grooming behavior within 27.7 minutes total assay time (n≥44). The mean is shown as a blue line, 95% confidence intervals for the mean are showed as dark shades. The median is shown as a dotted red line. 1 standard deviation is shown as light color shade. (C) Example ethograms of 15 individual *Canton S* flies in response to being shaken without or with dust generated by ABRS classifier. Each line is one individual. The color bar on the right stands for the color code used in the ethogram visualization. (D) Grooming progression for undusted or dusted *Canton S* flies. Behavior probabilities are calculated every 16 seconds in a sliding 32-second time window. Each data point is the average among all individuals (n≥44). The shade stands for the standard error of mean. (E) The ratio of anterior to posterior grooming of undusted and dusted flies in 150 s time window. The dash blue line indicates the mean value at the last time window.

2. The sensory organs contribute to grooming sequence

This chapter is adapted from published work: Neil Zhang, Li Guo, and Julie H. Simpson. "Spatial Comparisons of Mechanosensory Information Govern the Grooming Sequence in *Drosophila*." *Current Biology* (2020).

2.1 Introduction

Grooming helps insects get rid of fungi spores, parasites, and keep sensory organs clean. It has been shown that grooming can be induced by mechanosensation and taste in *Drosophila* [29,30].

In previous experiments [17], acute activation of multiple kinds of mechanosensory neurons on both anterior and posterior body parts induced anterior grooming, which persisted briefly after the light stimulus terminated. Intriguingly, the flies then transitioned to posterior grooming, suggesting that they retained a memory of the previous whole-body stimulation and acted upon the posterior stimulation once suppression from the anterior behavior ended. But it was unclear which type of mechanosensory neuron plays the most essential role in this optogenetically-induced sequence. In decapitated flies, bitter compounds and lipopolysaccharides (LPS, the component of Gram-negative bacteria

outer membrane) can initiate grooming through taste neurons stimulation [30]. But it was unclear whether grooming sequence can be induced. Here, I systematically determine the function of each sensory modality in grooming: mechanosensation, taste, olfaction and vision.

2.2 Results

2.2.1 Activation of mechanosensory bristle neurons across the whole body induces anterior grooming, followed by delayed posterior grooming

Mechanosensory bristles are the most abundant mechanosensory exteroceptors distributed all over the body. Bristle deflection induced by contact, air puff and parasites can induce targeted grooming [3,31,32]. I searched literature and image databases [33] to identify transgenic lines that target specific groups of sensory neurons and restrict expression further through split-Gal4 intersections [34]. I identified *Bristle-spGAL4-1* which specifically labels approximately half of bristle neurons distributed over the body (Figure 3B). Activating bristle neurons with light for one minute induced anterior grooming, while posterior grooming was observed immediately after light stimulus ended (Figure 3C). The grooming bout structures– the way body sweeps and leg rubs alternate – induced by dust and bristle neurons activation are also very similar. Flies alternate between head sweeps and front leg rubs during the optogenetic stimulation and between body sweeps and back leg rubs after stimulus termination. These results indicate that mechanosensory bristles may play an essential role in initiating the grooming sequence in dusted flies.

Bristle-spGAL4-1 labels a few neurons in the central nervous system (CNS), but grooming can be induced with targeted light on legs, abdomen or wings (which does

not activate CNS neurons). This suggests the sequential grooming was induced by bristle neurons rather than neurons in the CNS.

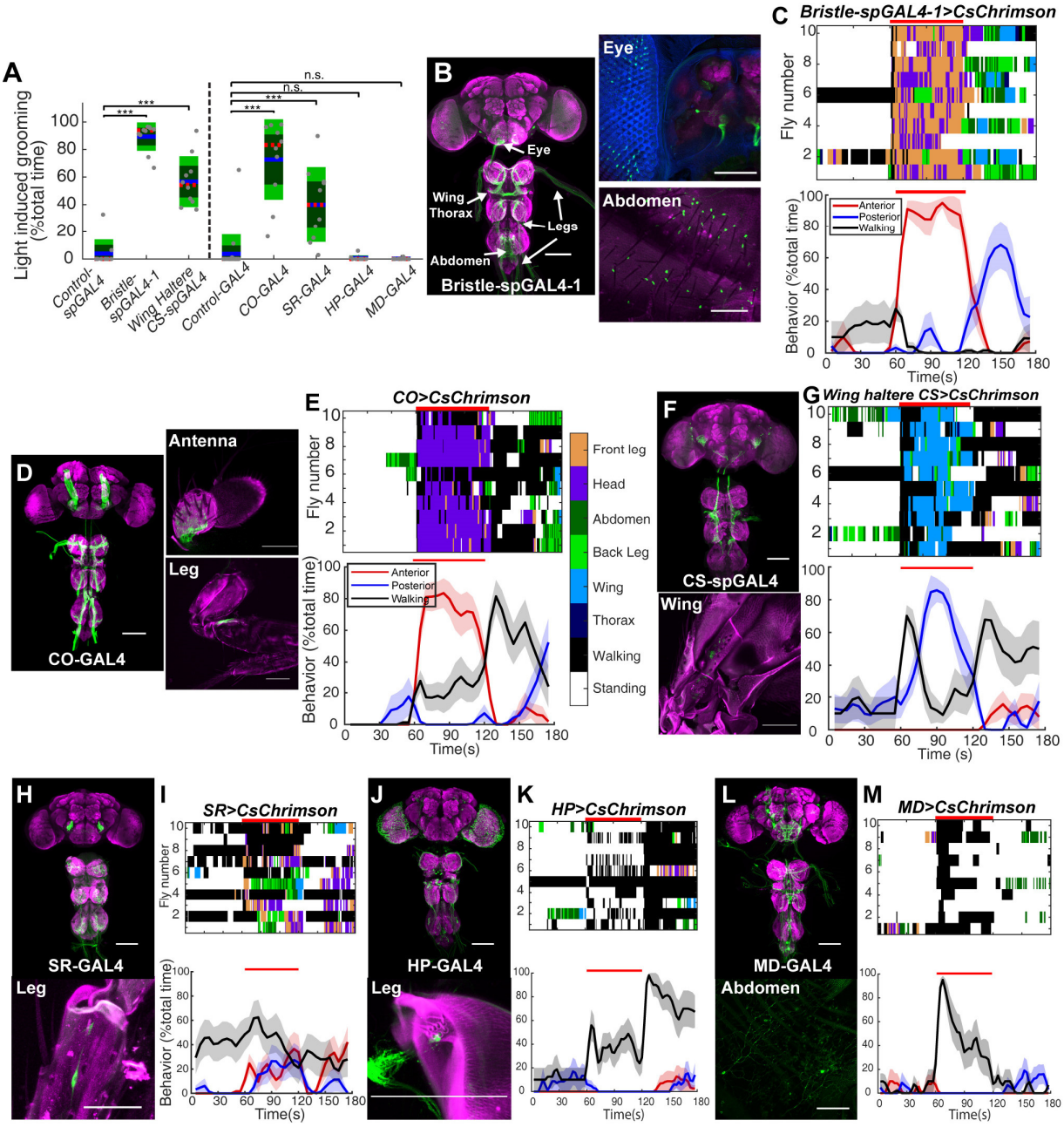

Figure 3. Grooming behavior can be induced by different mechanosensory neurons

(A) The percent of time flies spent in grooming during 1-minute optogenetic activation of different groups of mechanosensory neurons (n≥10). CO: chordotonal organ. CS: campaniform sensilla. SR: stretch receptor. HP: hair plate. MD: multidendritic neurons. (**B**) Expression pattern of *Bristle-spGAL4-1* in central

nervous system (CNS, left), eye (upper right) and abdomen (lower right). Green: anti-GFP. Magenta: anti-Bruchpilot in CNS, cuticle autofluorescence in abdomen. Eye facets are shown in blue. Scale bars, 100μm. (**C**) Grooming response induced by optogenetic stimulation of bristle neurons. Optogenetic stimulation was given between 60 and 120s, indicated by red line. Grooming progression is shown in the lower figure. Behavior probabilities over total time are calculated every 2.5 seconds in a 5-second time window. (**D**, **F**, **H**, **J**, **L**) The expression pattern of driver lines in central nervous system and peripheral nervous system. (**E**, **G**, **I**, **K**, **M**) Grooming response induced by light activation of different groups mechanosensory neurons. Optogenetic stimulation is indicated by red line. Data is plotted as descripted in Figure 3C.

2.2.2 Activating subgroups of chordotonal organs, campaniform sensilla and stretch receptors can also induce grooming movements, but not the sequence

Other types of mechanosensory organs respond to different mechanosensory stimuli. As described in chapter 1, the Johnston's organ detects sound, wind or contact [9,10]. Campaniform sensilla respond to deformation [35]. Chordotonal organs, hair plates and stretch receptors on the leg encode leg position and movement [4,11,14]. In principle, multiple types of mechanosensory organs may participate in grooming. Dust may be sensed by mechanosensory bristles to initiate grooming, while leg proprioceptors such as chordotonal organs and campaniform sensilla may provide position and pressure information required to target the legs accurately to specific body surfaces. It has been shown that grooming can be induced by optogenetic activation of antennal chordotonal organs and wing campaniform sensilla [29,36]. Here, I extended the study to include all types of mechanosensory organs. Upon 1-minute optogenetic activation through the red-light sensitive ion channel CsChrimson [37], grooming was induced by chordotonal organ neurons (CO-GAL4), campaniform sensilla neurons (Wing Haltere CS-spGAL4) and stretch receptor neurons (SR-GAL4). Activation of two other types of

mechanosensory neurons, hair plate neurons (HP-GAL4) and multidendritic neurons (MD-GAL4), did not cause grooming (Figure 3A).

However, the anterior-to-posterior grooming sequence was not induced by these three types of mechanosensory neurons: chordotonal organs induced head cleaning during light activation, and walking was observed immediately after light stimulus ended. Activating campaniform sensilla on wings and halteres together induced only wing grooming. Stretch receptors induced equal amount of anterior and posterior grooming. The alternation between body sweeps and leg rubs was not observed (Figure 3D-M). These data suggest that mechanosensory bristles are key for the normal grooming progression.

I also identified transgenic lines that target chordotonal organs and campaniform sensilla neurons on specific body parts (Figure 4). Antennal chordotonal organ activation induced antennal grooming, but activating leg or abdominal chordotonal organs did not induce grooming (Figure 4A, J). Activating haltere campaniform sensilla alone induced grooming directed toward the halteres and back leg rubbing. Activating campaniform sensilla on legs did not induce grooming (Figure 4A, K). Therefore, the same type of mechanosensory organ on different body parts play different roles in grooming.

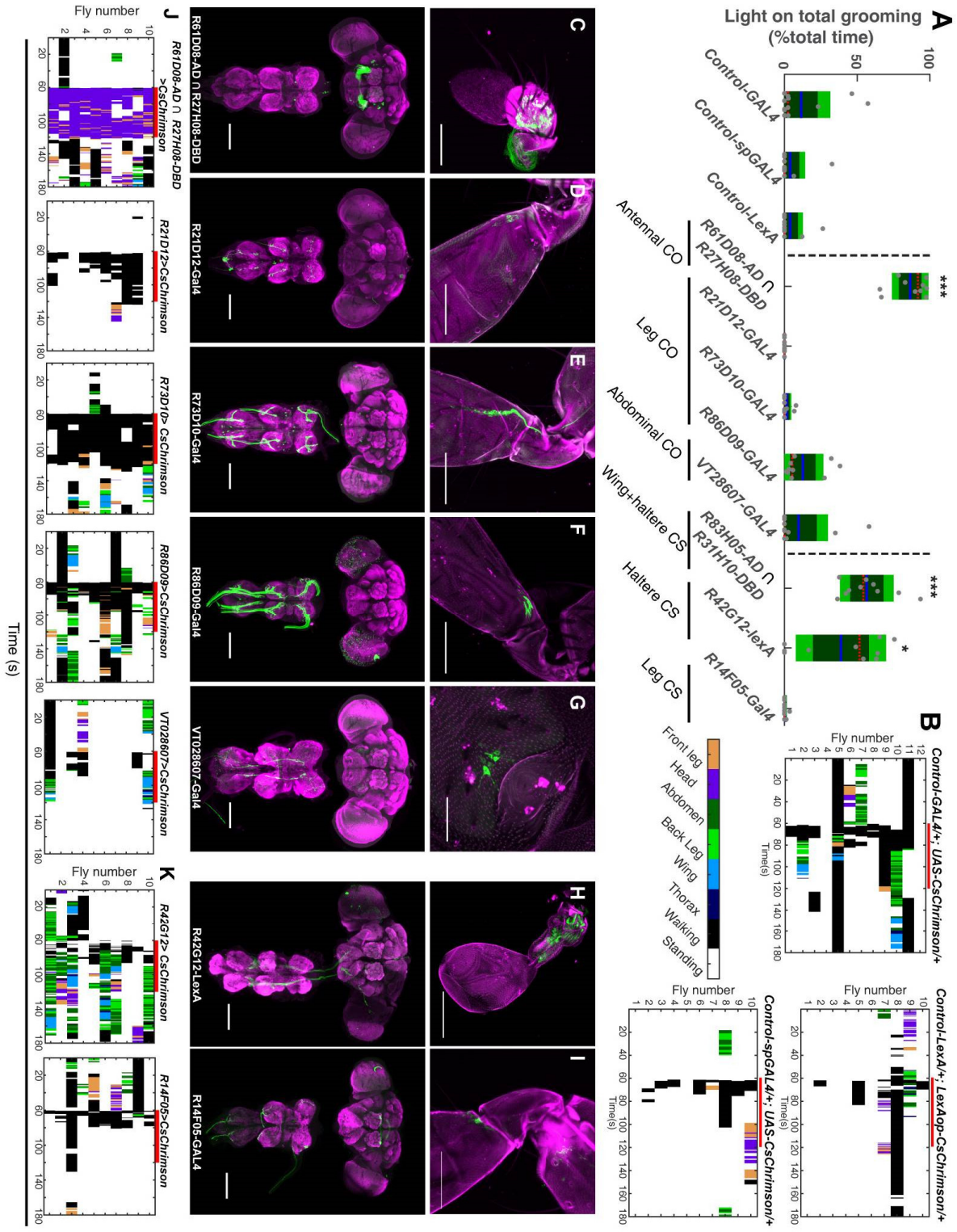

Figure 4. Grooming can be induced by subsets of chordotonal organs and campaniform sensilla on different body parts.

(**A**) The percent of total grooming induced by red light sensitive CsChrimson expressed in chordotonal organs or campaniform sensilla (n≥10). Wilcoxon rank-sum test was used to compare each line with the corresponding control line. Asterisks represent the following p values: *p < 0.05, **p < 0.01, ***p < 0.001. (**B**) Grooming ethograms of optogenetic stimulation in control flies. Red solid lines represent 1-minute light stimulus. (**C-I**) Expression patterns of driver lines targeting antennal (C), leg (D-F) and abdominal (G) chordotonal organs and haltere (H), leg (I) campaniform sensilla are visualized with mCD8-GFP in peripheral sensory organs and central nervous system. Magenta represents cuticle autofluorescence in peripheral sensory organs and neuropil (nc82 antibody) in central nervous system. Scale bars, 100μm. (**J**) Grooming ethograms of flies with optogenetic activation of different chordotonal organs. Red solid lines represent 1-minute light stimulus. (**K**) Grooming ethograms of flies with optogenetic activation of different campaniform sensilla. The expression pattern and grooming response of *Wing haltere CS-spGAL4* are shown in **Figure 3F, G**.

2.2.3 Sensory neurons inhibition indicates that multiple mechanosensory organs participate in dust-induced grooming

Gain-of-function experiments show that activation of these sensory neurons can induce grooming but do not demonstrate that these sensory neurons are the way flies normally sense dust. Loss-of-function experiments, in which flies are deprived of a sensory modality by genetic mutation or neuronal inactivation, would be ideal. Unfortunately, broadly inhibiting mechanosensory neurons usually causes lethality or extreme loss of coordination, masking specific grooming defects. To ameliorate this problem, I inhibited sensory neurons only on specific body parts.

Mechanosensory bristle neurons on the head or body may sense dust by bristle deformation. Even very small deflections can be detected by the mechanically gated ion channels located at the bristle base [7]. Alternatively, leg bristles might detect dust particles on other body parts during leg sweeps and rubs, either directly or as a difference in expected sweep force. Interommatidial bristles, located between each facet of the compound eye, are the most abundant bristle group, and their development can be disrupted by the P[*sev-wg*; w^-] insertion (Figure 5B) [38]. Flies

lacking eye bristles showed significantly reduced head grooming (Figure 5E). The whole compound eye can be eliminated by *so*^{D} or *eya*^{2} mutations (Figure 5C, D), and these eyeless flies also showed reduced head cleaning (Figure 5E). Since flies in the dark groom normally (Figure 6G, H), I attributed the reduced grooming phenotypes to loss of the interommatidial bristles. I also genetically silenced eye bristle neurons, using a split-GAL4 driver line I identified (Figure 5F) to express Kir2.1, an inward-rectifying potassium channel [39], but these flies did not show significant changes in head grooming (Figure 5G). Neuronal inhibition through tetanus toxin (TNT) or GtACR1 also did not cause head grooming defects (data not shown). When the eye bristles are missing, much less dust accumulates on the head, but the normal amount of dust is still there when the bristles are present with neurons silenced. Since dust on compound eyes may be sensed by both eye bristles and front leg mechanosensory bristles - stimulated during head sweeps - this may explain why inhibiting eye bristles alone did not reduce head cleaning: the signals from legs compensate. Since inhibition of leg bristle neurons decreases basal walking activity and limb coordination [5], it is difficult to address their specific contribution to grooming.

I also tested whether other mechanosensory organs are important for dust-sensing. Inhibiting antennal chordotonal organ neurons and wing campaniform sensilla neurons decreased grooming toward head and wings specifically (Figure 5G, H). These data demonstrate that multiple types of mechanosensory organs are involved in dust-induced grooming. Interestingly, inhibition of JO neurons by Kir caused a stronger phenotype than was seen in a previous study using TNT [36]. Since Kir inhibits neurons though membrane hyperpolarization, while TNT disrupts

the release of vesicles at chemical synapses [40,41], this difference suggests that the neurons in the JO may act through electrical synapses to promote grooming. Gap junctions have been observed between the JO and Giant Fiber [42]. Alternatively, JO neurons may just be less sensitive to TNT, as occurs in mushroom body neurons [43].

Our data provided evidence that although multiple mechanosensory organs participate in dust sensation, mechanosensory bristles play the most important role in grooming sequence. The loss-of-function data does not contradict this view, but the strongest evidence supporting it is that their activation induces normal grooming movements, and in an anterior-to-posterior sequence.

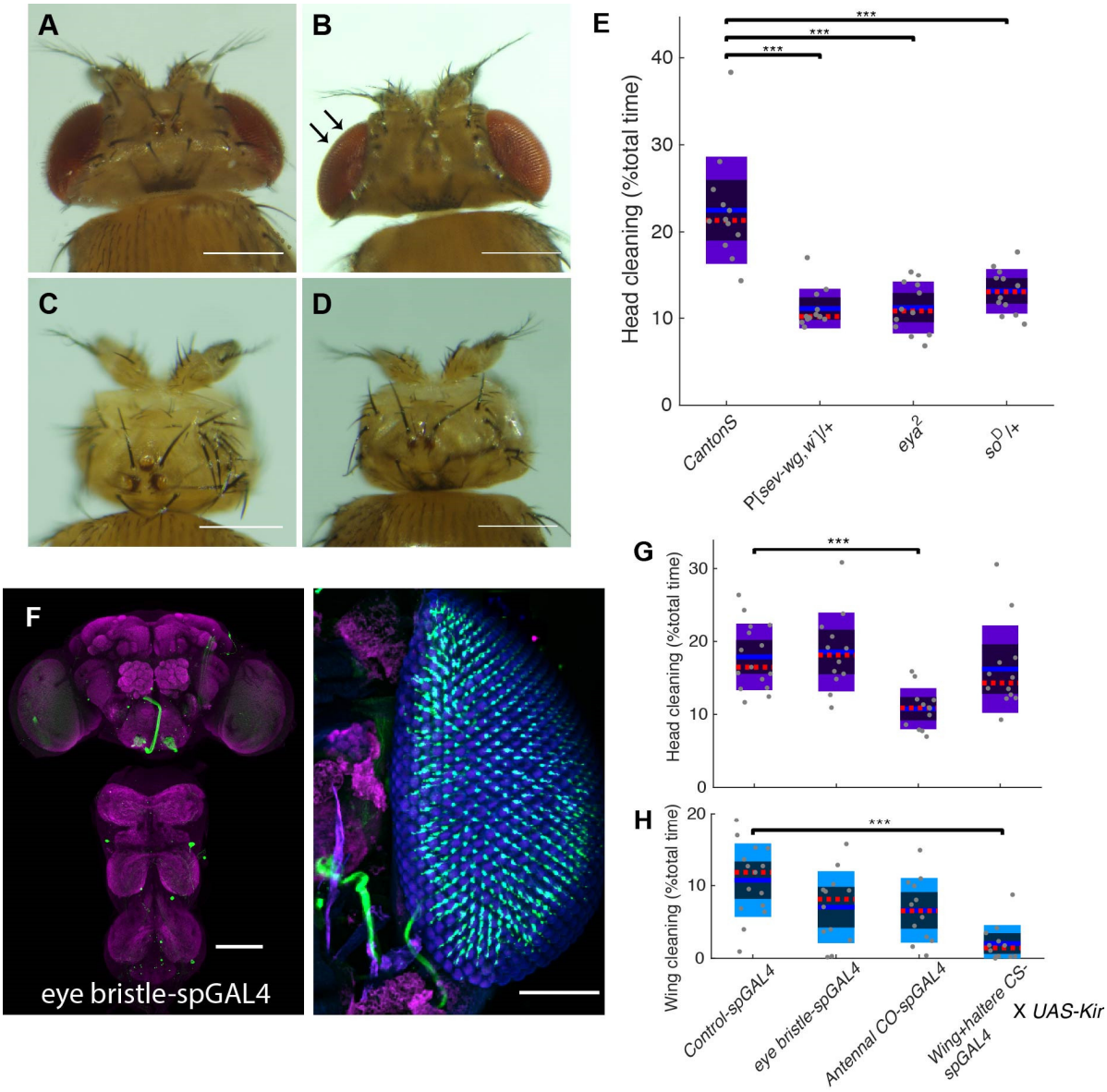

Figure 5. Multiple types of mechanosensory organs contribute to dust-induced grooming

Interommatidial bristles are visible in wild type *Canton S* eyes (**A**) but are absent in the P[*sev-wg*; *w*$^{+}$] mutant, as indicated by arrows (**B**). The *eya*^{2} (**C**) and *so*^{D} (**D**) mutants lack eyes entirely. Scale bars, 250 μm. (**E**) These mutants show reduced head grooming, as indicated by the percent of time dusted flies spent in head grooming within 27.7 minutes (n=12). (**F**) Expression pattern of *Eye bristle-spGAL4*. Green: anti-GFP. Magenta: anti-Bruchpilot. Eye facets are shown in blue. Scale bars, 100μm. (**G**) Inhibition of the neurons in the antennal chordotonal organs causes decrease in head cleaning while inhibition of wing campaniform sensilla (**H**) causes decrease in wing cleaning, as compared to the amount of cleaning displayed by the control flies (n≥12). Neurons were constitutively inactivated with *UAS-Kir2.1*.

2.2.4 The function of taste, vision and olfaction in grooming behavior

Stimulation of other sensory modalities, or disruption of expected stimulation, could also lead to grooming. I next investigated the function of gustatory, olfactory and visual organs in grooming.

Gustatory sensilla are important taste organs in fruit flies [44]. I optogenetically activated gustatory neurons that sense sweet, bitter or water with CsChrimson. Bitter taste neuron activation was reported to induce grooming [30] and I confirmed this finding (Figure 6A), but saw no anterior-to-posterior sequence (Figure 6B). Flies with a null mutation in a bitter receptor, Gr33a, did not show defects in grooming (Figure 6C), and inhibition of bitter taste neurons also did not cause grooming defects (Figure 6D). These data indicate that bitter taste is not necessary for dust-induced grooming. I tested different kinds of dust, from cornstarch to fungal spores, which presumably taste different, and observed sequential grooming (data not shown), further supporting that mechanosensory cues contribute more than taste to induce and organize grooming.

Grooming could help insects get rid of fungal spores attached to the cuticle. Fungi produce geosmin, sensed by the Or56a receptor, suggesting that olfaction could trigger grooming [45]. Antennal grooming may help insects maintain olfactory sensitivity [46]. Most conventional olfactory neurons are labeled by *orco-GAL4* driver line, but activating these neurons with CsChrimson did not induce grooming (Figure 6A). Two experimental manipulations were used to inhibit olfaction: an *orco* null mutant, and amputation of the third antennal segment and maxillary palps, where all olfactory receptors are located. Both types of anosmic flies groomed

normally in response to dust (Figure 6E, F), suggesting that olfaction is not essential.

Drosophila senses light with compound eyes and ocelli [47]. Flies could see dust on the eyes or the dust could interfere with expected visual signals. I conducted grooming experiments in the dark, recording videos with infrared light, and observed normal grooming movements and hierarchy: flies still performed anterior cleaning first (Figure 6G, H). This supports the assertion that vision is not essential to dust-induce grooming behavior and does not explain why the eyes are cleaned first.

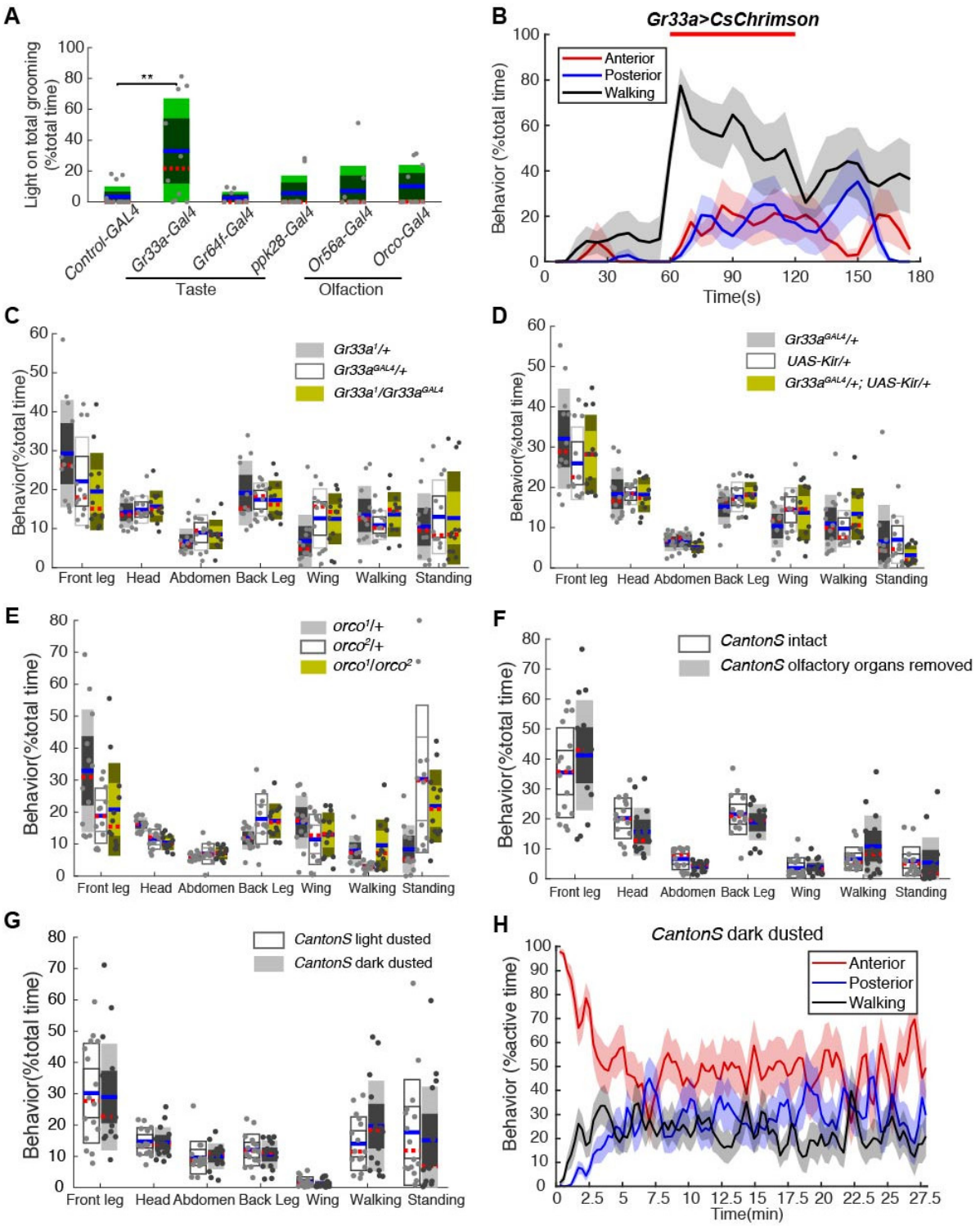

Figure 6. Taste, olfaction and vision are not necessary for dust-induced grooming.

(**A**) The percent of total grooming induced by 1-minute light activation to CsChrimson-expressing taste or olfactory neurons (n≥10). (**B**) Behavior probabilities induced by optogenetic activation of bitter taste neurons. Red solid lines represent 1-minute light stimulus. Behavior probabilities at different time points are quantified

as in **Figure 3C**. (**C**) Percent of time each behavior performed by dusted *Gr33a* null-mutant heterozygotes and control flies (n=12). No significant change was found between mutant and both controls. (**D**) Constitutive inhibition of bitter taste neurons did not change the amount of time flies spent performing each grooming movement (n≥11). (**E**) Percent of time each behavior was performed by dusted *orco* null-mutant homozygotes and control flies (n=12). No significant change was found. (**F**) Percent of time each behavior was performed by dusted *Canton S* with or without olfactory organs (n=12). No significant change was found. (**G**) Grooming in the light or dark did not change the amount of time flies spent performing each grooming movement (n≥12). (**H**) Behavior probabilities for dusted flies grooming in dark. Behavior probabilities at different time points are quantified as in **Figure 2D**.

2.3 Discussion

The neural mechanisms for processing sensory signals, and the way this information is used to select among behaviors, remain open questions. Evaluating which kinds of sensory inputs can initiate a behavior is the first step to understand this process. In this work, I systematically investigated the role of different types of sensory organs in *Drosophila* grooming. I found that multiple types of mechanosensory organs are involved in grooming, but mechanosensory bristles are most essential for grooming sequence: their activation induces the anterior-to-poster grooming progression and cyclic switching between body cleaning and leg rubbing. Electrophysiology recording have shown that a mechanosensory bristle can respond to displacements as small as 100nm [7]. Therefore, mechanosensory bristles could detect small deflections induced by dust particles. Johnston's organ also participates in dust sensing. JO C/E neurons can respond to movements as small as a few micrometers [9,10]. Thus, JO neurons could be activated by antenna displacements induced by dust weight. Parasites, mechanical irritants and damage will cause changes in the position and mechanical load of body parts which may be sensed by stretch receptors and campaniform sensilla. Grooming can help *Drosophila* remove debris, increase sensory acuity, and restore proper position of

body parts, so it is an appropriate response to mechanosensory stimulation. Future work will be required to determine the exact mechanism of dust sensing by different mechanosensory organs.

3. Iterative spatial comparisons of mechanosensory inputs is key for grooming sequence

This chapter is adapted from published work: Neil Zhang, Li Guo, and Julie H. Simpson. "Spatial Comparisons of Mechanosensory Information Govern the Grooming Sequence in *Drosophila*." *Current Biology* (2020).

3.1 Introduction

In dusted flies, sensory neurons on different body parts are activated at the same time. But flies only clean one body part at a time. Anterior grooming is usually chosen by the animal at the beginning. Our original grooming model postulated that the anterior dominance could result from (1) unequal inhibition between anterior and posterior grooming circuits or (2) differential sensory drive to different body parts. Here, I further investigate how anterior dominance can be affected by differential sensory drive. I also combined quantitative modeling with targeted optogenetic activation to investigate how changing mechanosensory input contributes to the change of behavior choice over time. Two terms describe the anterior-to-posterior grooming sequence: *hierarchy* and *progression*. *Hierarchy* refers to which body part is groomed first or which is selected when there is competition. *Progression* represents the change in the choice of grooming actions over time.

3.2 Results

3.2.1 Modeling indicates that unequally-distributed mechanosensory stimulation, changing with time, can account for sequential grooming

First, I developed a computational model to explain the grooming sequence in dusted wildtype flies. In our model, sensory organs all over the body are activated

by dust simultaneously, but only one pair of legs can be used at a time. At each simulated grooming iteration, the body part which has the strongest sensory input is selected and cleaned. Since grooming removes dust, the drive to the selected body part is reduced, which may lead to a change of behavioral choice at the next evaluation. Our model has two layers: the sensory layer quantifies dust-induced sensory input from different body parts. The winner-take-all layer compares sensory input strengths and selects one grooming subroutine for execution, thus converting probabilistic sensory inputs into a single behavioral output. Three variables are used in the sensory layer: ***d(t)*** represents the amount of dust on each body part. ***a(t)*** represents the sensory input induced by dust. ***a(t)*** follows a normal distribution whose mean is equal to current ***d(t)***. ***dr*** indicates the dust removal rate, or the percentage of dust that is transferred from a body part to the legs in each grooming bout. It is defined as a percentage of the current ***d(t)*** rather than a constant amount to capture diminishing returns – less dust is removed when there is less on a body part. The initial value of ***d(0)*** and the constant value for ***dr*** are specified by the user, and first iteration selects the body part with the highest ***a(0)*** to be groomed. ***d(t)*** is re-calculated in each iteration, using ***dr*** applied to the currently selected body part to reduce ***d(t)*** and determine new values of ***a(t)*** for each body part. The winner-take-all layer then compares the updated sensory input level ***a(t)*** to select the next grooming action (Figure 7A). (Note that I did not model grooming bout durations here; these were drawn from the distribution obtained in experimental data.)

Sensory input levels should be a combination of the amount of dust and the number of bristles that detect it. To model the grooming sequence in wildtype flies, I assumed that each bristle gets the same amount of dust and set up initial dust

distribution according to number of bristles on each body part: the head has ~1200, the abdomen has ~600, and the wings have ~400 [48–50]. This initial dust distribution reproduces the anterior grooming dominance observed in dusted wildtype flies. I also tested different values of ***dr,*** the dust removal rate. A simulation with ***dr***=0.2% generates a similar speed of grooming progression to what I observed in real flies. Anterior and posterior grooming probabilities became equal at the end of the simulation (Figure 7B), as they do when dusted flies reach “steady state”. Therefore, sequential grooming can be modeled by setting the initial sensory input strength to different body parts based on their number of mechanosensory bristles and then varying the subsequent drive based on targeted dust removal.

This model gives us guidance about how the grooming sequence can be affected by sensory inputs. With the help of model simulation, I next designed experiments to test how hierarchy and progression are affected by sensory inputs.

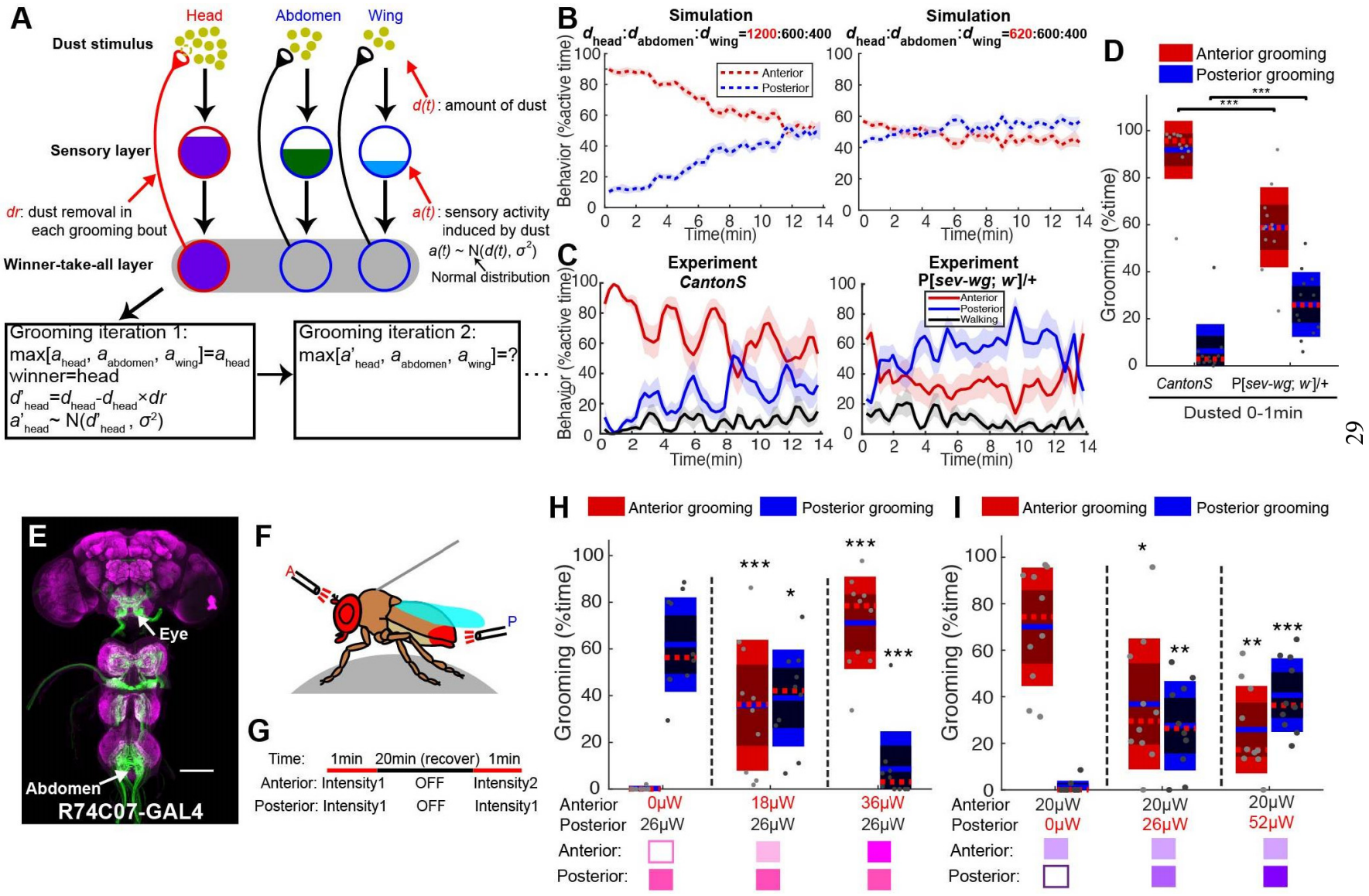
A
Head
Abdomen
Wing
Dust stimulus
Sensory layer
dr: dust removal in each grooming bout
Winner-take-all layer
d(t) : amount of dust
a(t) : sensory activity induced by dust
a(t) ~ N(d(t), σ²)
Normal distribution
Grooming iteration 1:
max[a_head, a_abdomen, a_wing]=a_head
winner=head
d'_head=d_head-d_head×dr
a'_head~ N(d'_head , σ²)
Grooming iteration 2:
max[a'_head, a_abdomen, a_wing]=?
B
Simulation
d_head:d_abdomen:d_wing=1200:600:400
Simulation
d_head:d_abdomen:d_wing=620:600:400
Anterior
Posterior
Behavior (%active time)
Time(min)
C
Experiment
CantonS
Experiment
P[sev-wg; w-]/+
Anterior
Posterior
Walking
D
Anterior grooming
Posterior grooming
Grooming (%time)
CantonS
P[sev-wg; w-]/+
Dusted 0-1min
E
Eye
Abdomen
R74C07-GAL4
F
A
P
G
Time: 1min 20min (recover) 1min
Anterior: Intensity1 OFF Intensity2
Posterior: Intensity1 OFF Intensity1
H
Anterior grooming
Posterior grooming
Grooming (%time)
Anterior 0μW 18μW 36μW
Posterior 26μW 26μW 26μW
Anterior:
Posterior:
I
Anterior grooming
Posterior grooming
Grooming (%time)
Anterior 20μW 20μW 20μW
Posterior 0μW 26μW 52μW
Anterior:
Posterior:

Figure 7: The hierarchy of grooming movements is determined by sensory input strengths to different body parts
(**A**) Schematic of grooming model with varied initial sensory inputs to different body parts. Dust (***d(t)***) activates sensory organs on different body part. Flies groom the body part with highest sensory activity (***a(t)***). The sensory activity term (***a(t)***), which represents a combination of amount of dust and number of sensory neurons, follows a normal distribution whose mean is ***d(t)***. For each grooming iteration, the value of the term ***d(t)*** updates, as some percent of dust (***dr***) is removed from the body part that won the previous iteration. The change of dust distribution drives the sequential progression of grooming. (**B**) Model simulation with different initial dust levels. Left: Initial dust levels were set up according to bristle numbers on different body parts in wild-type files. Right: Simulation with decreased anterior sensory input reduced the initial ratio of anterior to posterior grooming. (**C**) Different grooming hierarchies were observed in dusted *Canton S* or P[*sev-wg*; *w*$^{-}$]/+ flies that lack eye bristles (n=12). Data is plotted as descripted in **Figure 2D**. (**D**) Quantification of the amount of anterior and posterior grooming during the first minute in dusted *Canton S* and P[*sev-wg*; *w*$^{-}$]/+ shows that changing the number of eye bristles alters the initial amount of anterior grooming relative to posterior, lowering the A:P grooming ratio. (**E**) Expression pattern of *R74C07-GAL4* in eye bristle neurons that project to the SEZ, as well as posterior abdominal bristles that innervate the ventral nerve cord (VNC). Scale bars, 100μm. (**F**) Schematic of “fly-on-a-ball” system. For optogenetic stimulation, two light fibers target anterior and posterior body part separately. (**G**) Protocol used in optogenetic competition assay. Each fly was tested in two 1-minute light stimulations. For each stimulation, the same posterior light (or anterior light) was coupled with different anterior light (or posterior light). 20 minutes recovery time was given between the two stimulations. (**H-I**) The change of grooming hierarchy as a result of varied sensory inputs (n=10). (**H**) In tethered *R74C07>ChrimsonR* flies, posterior light stimulus was kept constant while anterior light stimulus was increased in different experiments. An increased ratio of anterior to posterior grooming was observed. (**I**) When the anterior light stimulation level was held constant and the competing posterior light levels were increased, a decreased ratio of anterior to posterior grooming was observed.

3.2.2 The anterior:posterior sensory input ratio dictates grooming hierarchy

The grooming hierarchy can be observed by the A:P grooming ratio – the relative amounts of anterior and posterior grooming as described in Figure 2E. In our simulation, this ratio is affected by sensory input strength, and so reducing initial dust values for the head led to decreased anterior grooming (Figure 7B). The predictions of the model led us to devise additional experimental tests. It has been

challenging to apply specific amounts of actual dust to fly body parts, but there are several alternatives. First, I lowered sensory input to the eye by applying dust to mutant flies lacking eye bristles. Both the amount of dust retained on the eyes, and the sensory neurons that detect it, were reduced. This resulted in reduced initial A:P grooming ratio (Figure 7C, D) and supports our prediction that sensory input strengths establish anterior dominance in the hierarchy.

Optogenetic experiments with light aimed at specific body parts allow us to control sensory input strength with more accuracy. I expressed ChrimsonR [37] in mechanosensory bristle neurons, tethered the fly, and then used two independently targeted light sources to separately activate anterior and posterior body parts (Figure 7F). *R74C07-GAL4* labels mechanosensory bristle neurons on eyes and posterior abdomen (Figure 7E), providing better separation of the activation zones. I gave the same fly two different 1-minute light activation protocols, and compared grooming behaviors induced by different light conditions (Figure 7G). In the first set of experiments (Figure 7H), for each pair of light presentations, I held the posterior light intensity constant and varied the level of anterior stimulation. The posterior activation is sufficient to induce posterior grooming in the absence of competition, but higher levels of anterior activation drove an increase in anterior grooming at the expense of posterior grooming. In the second set of experiments, the same anterior illumination level was paired with different posterior stimulations. High posterior light levels were enough to swing the balance toward posterior grooming (Figure 7I). Previous studies showed that animals perform input comparison between left and right sensory organs [51,52]. Our model simulation suggested that spatial sensory comparison between anterior and posterior body parts is also an essential part of

behavior choice. By using classical genetic mutants and a novel optogenetic assay, I experimentally demonstrated this prediction: the initial grooming hierarchy is determined by the ratio of sensory input strength to different body parts.

3.2.3 Grooming progression is absent during constant sensory stimulation

Flies remove dust particles from specific body parts during grooming. In our model, I simulated this by including a term for dust removal (***dr***). This removal, and the corresponding change in the distribution of sensory inputs, is critical for the progression of grooming action choice: when I set dust removal to zero in the simulation, there is no anterior-to-posterior grooming progression (Figure 8A). The probabilities of anterior and posterior grooming stayed constant and corresponded to their initial activation levels (***a***): when the A:P sensory input ratio was high, anterior grooming always dominated, and when the A:P sensory input ratio was low, posterior behaviors dominated over the whole time-course.

I then used both genetic reagents and mechanosensory competition experiments to test this prediction. First, I gave bristle neurons distributed over whole body (*Bristle-spGAL4-1*) constant optogenetic stimulus for 14 minutes (in undusted flies). The ratio between anterior and posterior grooming stayed similar over time (Figure 8B). I identified *Bristle-spGAL4-2* that targets bristle neurons on the body and legs but not eye bristle neurons (Figure 8C, D). Activating these neurons mainly induced posterior grooming (Figure 8E). Regardless of the starting stimulation ratio, under constant illumination, no obvious grooming progression was observed. The fly-on-a-ball set up gave us more freedom to separately control the sensory inputs to different body parts. Using the *R74C07-GAL4* line, I tested 5-minute constant light stimulus in three conditions: high anterior light intensity, similar

anterior and posterior light intensity and high posterior light intensity. The ratio of anterior:posterior grooming behavior was determined by the initial anterior:posterior sensory input ratio and stayed constant over time in all three conditions (Figure 8F-H). These results confirmed our previous conclusion that the grooming hierarchy is determined by the ratio of sensory input strengths from different body parts, and demonstrated that the change of sensory stimulation over time is necessary for grooming progression. But what aspect of the dynamics are the flies measuring to determine which body part to groom as time goes on?

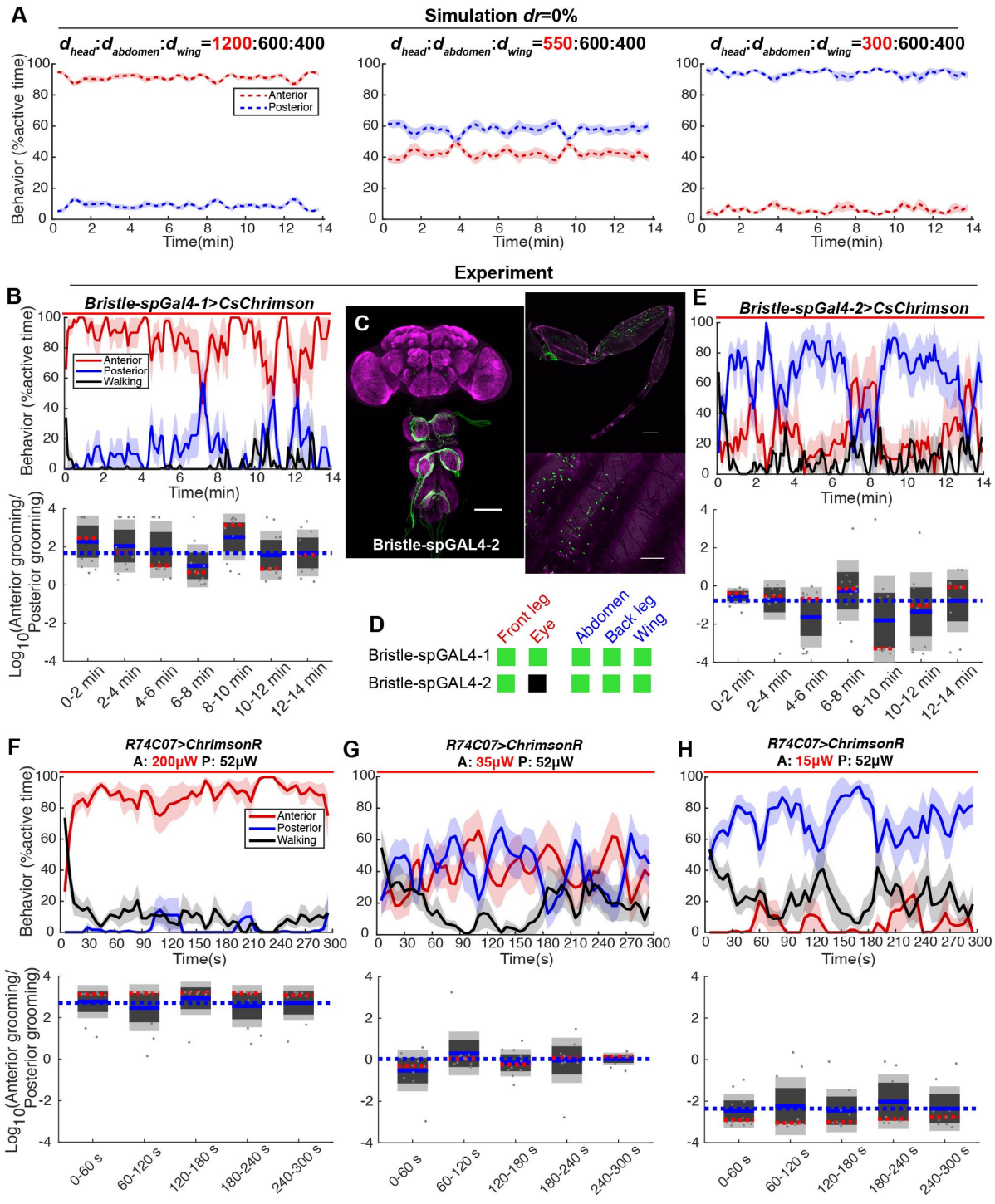

Figure 8. Grooming progression requires changing sensory stimulus

(**A**) Model simulation with constant dust levels over time (*dr*=0%). Data is plotted as descripted in **Figure 2D**. (**B**, **E**) Using spGAL4 lines to restrict expression of CsChrimson to mechanosensory bristle neurons on different body parts and applying light from below to freely-moving flies (n=10). The probability of anterior grooming (red), posterior grooming (blue), or walking (black) is calculated every 5

seconds in a 10-second time window. Below, the ratio between anterior and posterior grooming is calculated in 2- minute time windows. The blue dashed line indicates the mean value for the last time window. No significant difference was found between each time window (Kruskal–Wallis test). (**C**) Expression pattern of *Bristle-spGAL4-2* visualized with *UAS-mCD8-GFP* in CNS, leg and abdomen. Scale bars, 100 μm. (**D**) Summary table of expression patterns of two bristle neurons spGAL4 lines. Green indicates expression, black indicates no expression. The detail expression pattern of *Bristle-spGAL4-1* can be found in Figure 3B. (**F**-**H**) In tethered *R74C07>ChrimsonR* flies, constant level anterior and posterior light stimulus was given for 5 minutes (n=10). Behavior probabilities and anterior to posterior grooming ratio is quantified as in **B**.

3.2.4 The timing of grooming progression depends on changing sensory inputs

To investigate how the change of sensory inputs affects grooming progression, I performed simulations with different dust removal (***dr***) values. Increasing the rate of dust removal shifted the time at which the posterior grooming percentage overtakes anterior earlier, indicating faster progression (Figure 9A). The time point when a fly has finished half of the total anterior grooming it will do is also a measure of the grooming progression speed. Flies with larger dust removal values progress to posterior grooming faster, resulting in earlier anterior “half-times” (Figure 9B).

I used the “fly-on-a-ball system” to test predictions from simulation. Targeting light to anterior and posterior body parts allows us to control the relative sensory inputs and vary their intensity over time. I tethered *R74C07>ChrimsonR* flies and applied a very gradually decreasing posterior light stimulation selected to be sufficient to induce posterior grooming in the absence of competing stimuli (Figure 9D). I coupled this posterior stimulation with two different anterior light intensity ramps. When the anterior light levels decreased slowly at the beginning and fell under posterior light levels late (red, slow ramp), flies reached the anterior and posterior grooming equilibrium point ~270 s and achieved “half-time” around 120 s.

When the anterior light levels decreased faster at the beginning and fell under posterior light levels earlier (purple, fast ramp), flies transitioned to predominantly posterior grooming sooner (180 s) and achieved half-time at 90 s (Figure 9C, F). An alternative way to quantify the grooming progression is to examine the ratio of anterior to posterior grooming in sequential 60 s time bins. The A:P grooming ratios shift significantly at 60 s with a faster anterior ramp but only after 180 s with the more gradual one (Figure 9E). The faster decrease in anterior stimulation levels mirrors the higher dust removal values in the simulation (Figure 9A right panel), and may mimic more efficient dust removal in dirty flies. Therefore, the way the relative sensory inputs change influences the timing of grooming progression.

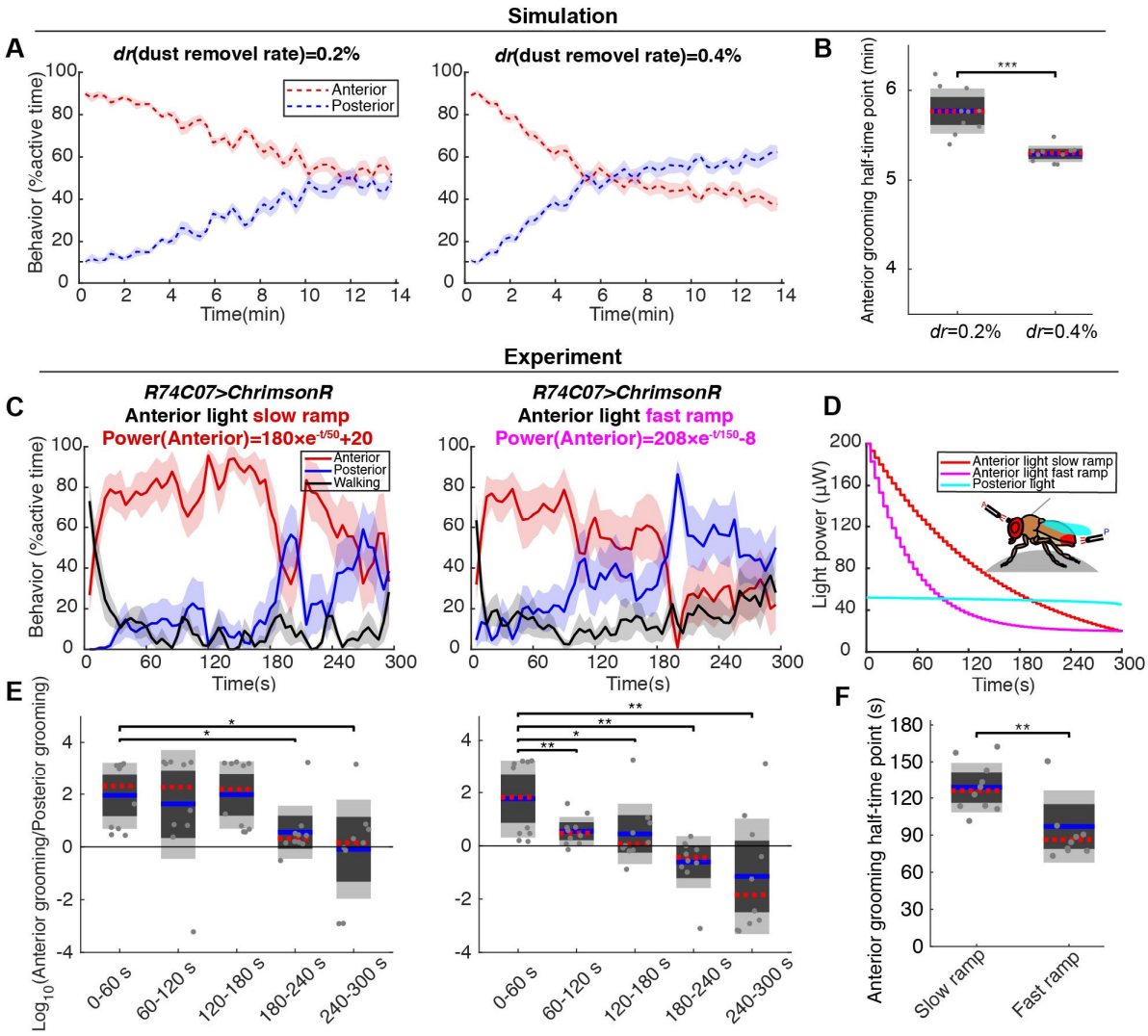

Figure 9: The timing of grooming progression depends on changing sensory inputs

(**A**) Model simulation with different dust removal rates shows that the transition to higher probability of posterior grooming occurs earlier when the dust removal rate is higher, (as in Figure 7B, d_{head} = 1200, $d_{abdomen}$=600, d_{wing}=400; each simulation was performed 10 times). Data is plotted as descripted in **Figure 2D**. This is also quantified in **B** as the time points at which simulation flies finish half of their total anterior grooming. (**C**-**F**) Tethered *R74C07>ChrimsonR* flies were tested in two different light ramps. In different experiments, the same light ramp was given to posterior body parts, while a slow or fast light ramp was given to the anterior body parts (n=10). (**C**) Behavior probabilities are quantified as in **Figure 8B**. (**D**) Light conditions used in the experiments. (**E**) Quantification of ratio between anterior and posterior grooming in each 60s-time window. (**F**) The anterior grooming half-time points under different light conditions.

3.2.5 Iterative spatial comparisons of mechanosensory inputs, rather than temporal comparisons showing anterior dust removal rate, is key for grooming sequence

Two possible mechanisms can explain the result that faster anterior light decrease leads to faster progression. First (1), faster sensory input change reduces the anterior: posterior sensory input ratio faster. Flies may frequently compare the levels of sensory input to anterior vs. posterior body and switch when they become close to equal. Animals respond to the absolute level of sensory inputs, but they also monitor how these sensory inputs change over time [53–55]. An alternative mechanism (2) is that flies may measure the temporal change of sensory input to a specific body part. Faster anterior sensory input change indicates more efficient anterior grooming, which may drive the grooming progression to posterior body parts (Figure 10A). I designed optogenetic competition experiments to investigate which spatial and temporal comparisons contribute to the grooming sequence and thus discriminate between these possible mechanisms.

As shown above, initial grooming movement choice is determined by initial anterior: posterior sensory input ratio. I further tested whether flies perform iterative spatial comparisons throughout the whole grooming sequence. I applied the same anterior stimulation (decreasing with an exponential function) in competition with either low (dark blue) or high (light blue) posterior stimulation levels (Figure 10B). In both light conditions, anterior grooming dominated initially, as flies almost exclusively performed anterior grooming during the first 50 s (Figure 10C). If the amount of anterior stimulation relative to posterior stimulation (A:P input “ratio”) is important, then flies in the “high-posterior” case should transition first. Alternatively,

if the rate at which anterior stimulation decreases (temporal comparison) is the only key criteria for transition, the flies should show the same grooming progression in both experiments since the same anterior light protocol was used. The former was what I saw, indicating that “ratio” is important. In low-posterior case, anterior grooming dominated over posterior grooming for the whole 300 s. In high-posterior case, posterior grooming successfully out-competed anterior grooming at 30μW:52μW, which I call the “equilibrium point” (Figure 10C). *R74C07-GAL4* labels more eye bristle neurons compared with abdominal bristle neurons, which may explain why lower anterior light intensity compared with posterior light is required to reach equilibrium. The different “half-times” of 90 s vs. 125 s (Figure 10D) also indicate that faster progression was induced by high posterior light stimulus. Therefore, flies not only compare the initial sensory input to different body parts, but also make iterative spatial comparisons throughout grooming. This iterative spatial comparison is essential for the change of behavior choice.

Next, I used this “equilibrium point” (30μW:52μW) (Figure 10B, C) to test whether the behavior choice can also be affected by the temporal comparison of sensory inputs to the anterior region. I gave flies constant posterior light intensity and presented different anterior stimulus protocols that ramped through the equilibrium point (indicated by arrow) at different slopes (Figure 10E). Interestingly, the transition times from majority anterior grooming to majority posterior grooming happened at almost the same time (150 s) in both conditions (Figure 10F). An alternative measure of behavior choice, the A:P grooming ratio around that point, also showed no significant difference (Figure 10G). This indicates that this temporal

comparison – the rate of change of anterior mechanosensory input - is not critical for the grooming progression.

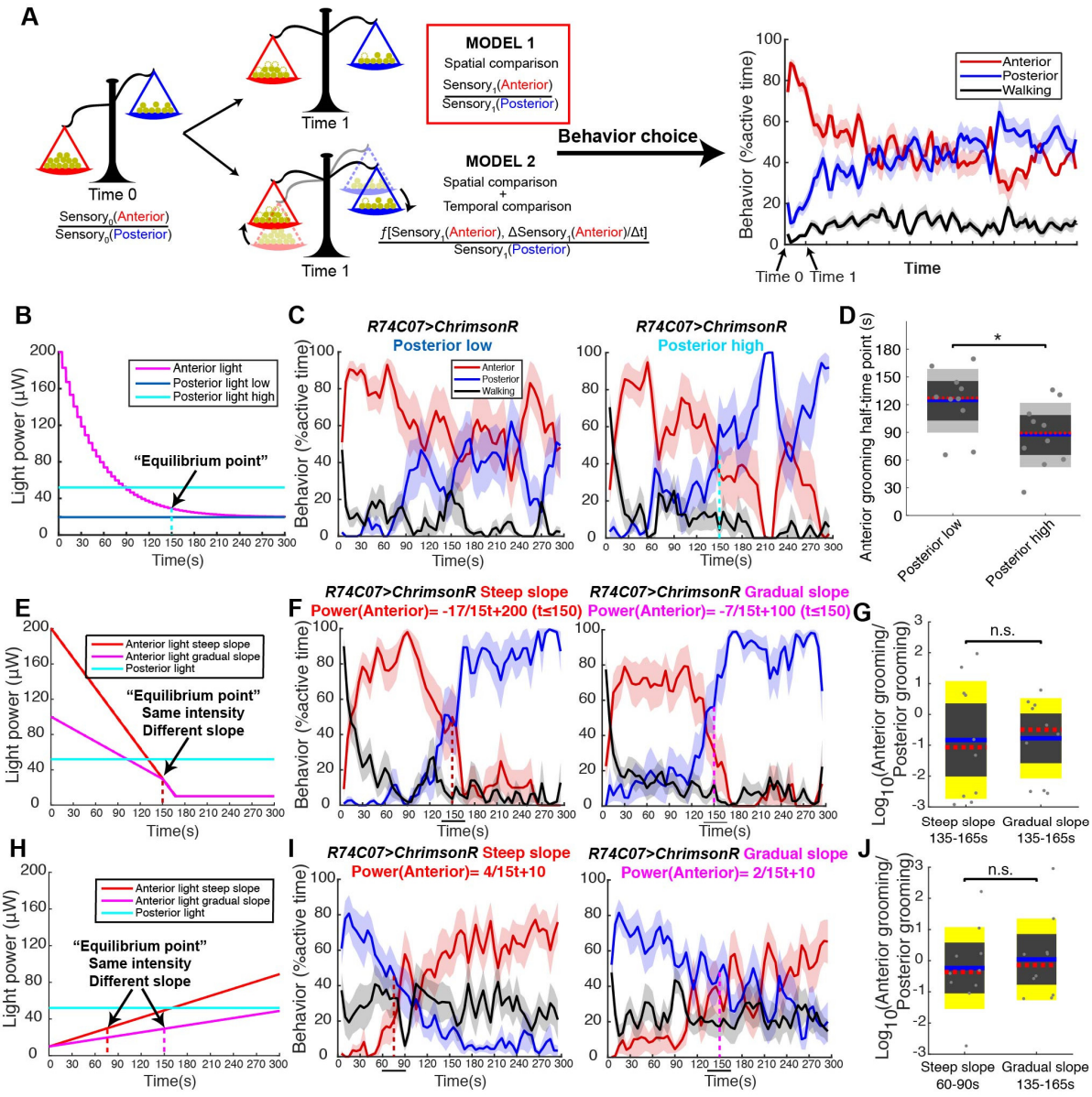

Figure 10: **The changing ratio of sensory input strengths to different body parts, rather than the rate of change of anterior sensory input, is key for the progression of grooming**

(**A**) Two different models can explain how the change of sensory inputs drives the change of behavior choice. In the first model, only the ratio of sensory input strengths to different body parts determines the behavior choice at that time point. In the second model, both the sensory input ratios and the temporal change of sensory information are important. (**B-D**) Tethered *R74C07>ChrimsonR* flies were tested in two light conditions. In each condition, different level of posterior light was

coupled with same anterior light curve (n=10). The “equilibrium point” (30μW:52μW) in posterior high condition where the probability of anterior grooming equals to posterior grooming is shown by a light blue dashed line. (**B**) Change of light power over time in each experiment condition. (**C**) Behavior probabilities at different time point is quantified as in **Figure 8B**. (**D**) The anterior grooming half-time points under different light conditions. (**E-J**) In different experiments, same constant light was given to posterior body part; anterior light crossed the same “equilibrium point” (30μW:52μW, indicated by arrow) at different slopes (n=10). Vertical dashed light indicates the position of “equilibrium point”. (**E, H**) Change of light power over time in each experiment condition. (**F**, **I**) Behavior probabilities at different time point is quantified as in **Figure 8B**. (**G**, **J**) The ratio of anterior grooming to posterior grooming within the 30 s time windows around the target light intensity point. The time windows are indicated by black solid lines in **F**, **I.**

The anterior to posterior grooming transition occurs when the sensory input ratio reaches a certain threshold– but does the history matter at all? I tested whether reversing the ramp of anterior stimulation would alter the transition point, starting with low anterior illumination and increasing it to approach the equilibrium point (30μW:52μW; two black arrows) from below at different time points, using various slopes (Figure 10H). I found that A:P grooming ratios were similar at that target point, regardless of how it was approached (Figure 10I, J). Thus, I demonstrate that the slope value and sign do not affect grooming movement choice, but that the current ratio of anterior to posterior sensory input, which changes over time, is the essential determinant. I conclude that iterative instantaneous spatial comparisons between sensory inputs to different body parts drive changing grooming movement choice over time, leading to an anterior-to-posterior grooming sequence in dusted flies.

3.3 Discussion

The central nervous system integrates information from different sensory modalities and body parts. Our experiments show that during grooming, flies frequently compare sensory input strengths from anterior and posterior body parts

to choose grooming actions. Mechanosensory bristle and proprioceptive neurons in the leg extend axons into distinct areas of the leg neuropils of the ventral nerve cord. Bristle neurons from the body also project to the ventral nerve cord and abdominal bristle neurons arborize in the abdominal ganglia [5], while interommatidial bristle neurons and head bristle neurons extend primarily into the subesophageal zone of the brain (Figure 11). Sensory and motor neurons have been characterized, and some interneurons that receive sensory neuron inputs from the left and right legs have recently been identified [8], but the majority of interneurons that compare sensory inputs from different body parts remain to be found.

Behavioral analyses suggest challenges the nervous system solves. For grooming, the presence of a somatotopic map can be inferred because of the precision with which the legs move to sweep stimulated bristles [31]. Some ability to ignore self-generated sensory stimulation also seems likely, since flies do not get stuck in constant grooming loops triggered by bristle deflections during their own leg sweeps. Interhemispheric neurons may coordinate in-phase and out-of-phase leg movements for symmetric body sweeps and asymmetric leg-rubs. Intersegmental neurons mediate mutual exclusivity between front and back leg movements to maintain posture and balance.

Modeling guided experimental designs for our optogenetic competition assay. I determined which spatial and temporal comparisons matter for behavior choice. For grooming, I now know that comparisons between mechanosensory bristle neurons on anterior and posterior body parts are critical. Sensory integration and action selection are common challenges animal brains must solve to coordinate effective

behaviors. Demonstrating the behaviorally-relevant comparisons is the first step to mapping the circuit motifs that accomplish them.

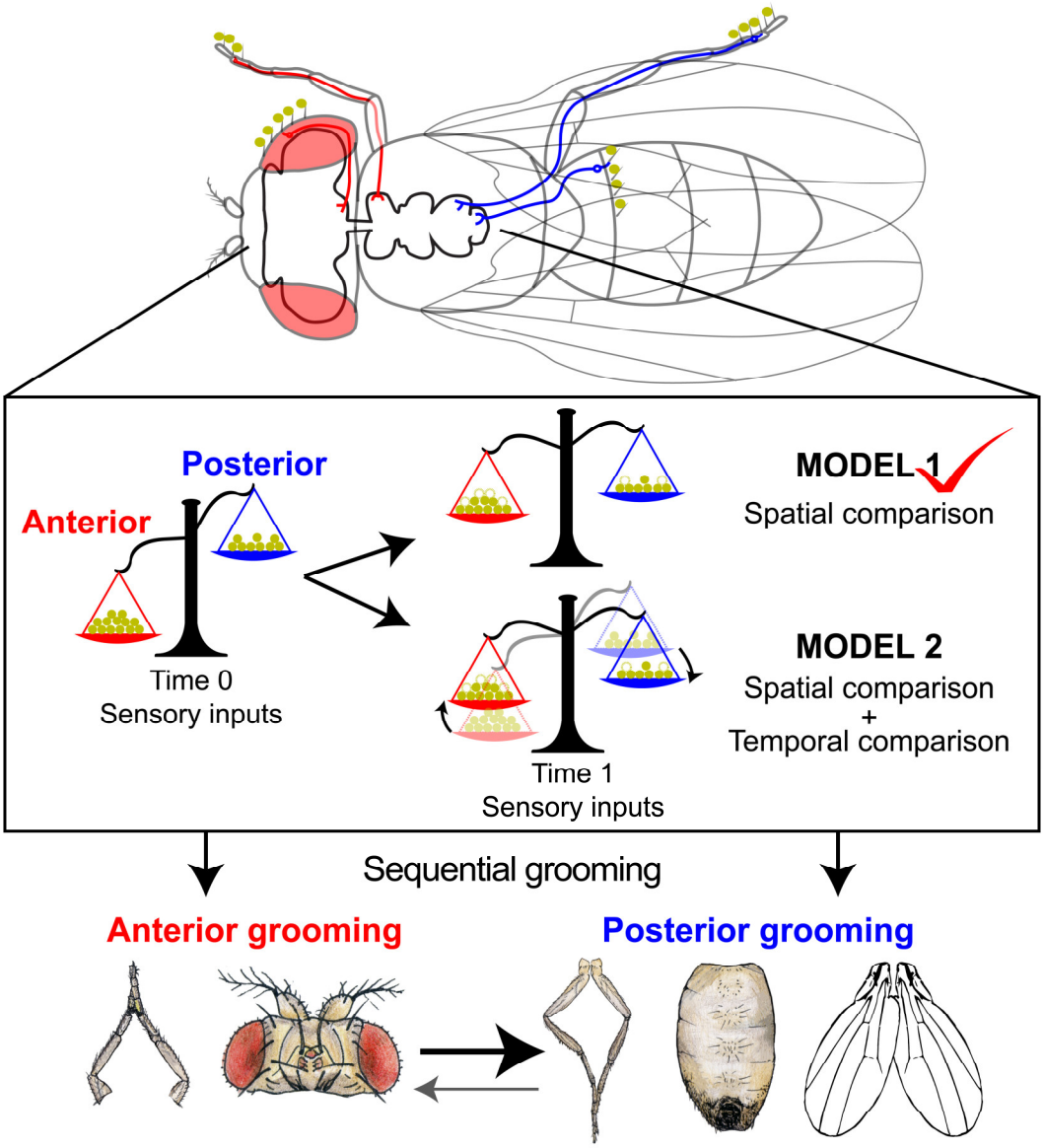

Figure 11. Graphical summary of the model
Dust is sensed by mechanosensory bristles across the body. Flies perform spatial comparison of sensory inputs between anterior and posterior body parts and clean the body part which has the highest sensory input. Grooming changes the spatial distribution of sensory inputs. This updating spatial comparison, rather than the rate of dust removal from the anterior drives the anterior-to-posterior grooming sequence.

4. Characterization of wing campaniform sensilla downstream neural circuits in wing grooming

4.1 Introduction

Our experiments show that the spatial comparison of mechanosensory information plays a key role in grooming sequence. Next, I will investigate the neural circuits that process mechanosensory inputs. Using a combination of anatomically guided selection of genetic reagents and behavioral screening, we previously mapped much of the neural circuitry controlling antennal grooming [36]. I will employ similar approach to identify the neural circuit that controls wing grooming (a posterior grooming behavior) and mediates the selection among anterior and posterior cleaning routines.

Various tools have been developed for dissection of neural circuits. Electron microscopy (EM) is the gold standard for synapse detection. The EM reconstructions of *Drosophila* larval CNS and adult brain have helped researchers map neural circuits of nociception, vision and olfaction [56–58]. However, the complexity of EM image volumes often brings challenges for data analysis. Alternative methods, such as herpes simplex virus-based anterograde tracers have been widely used in mammals [59]. A recently developed genetic tracer, *trans*-Tango [60], makes it possible to perform anterograde neural tracing in *Drosophila*. Besides these anatomical methods, functional mapping tools are also essential for identifying neural circuits recruited to a specific behavior. By activation or inhibition screens using thousands of transgenic neural lines, researchers have identified

circuit components involved in behaviors such as walking, grooming and aggression in adult flies [61].

In this study, I will combine both anatomical and functional methods to investigate the downstream neural circuits of wing grooming. A previous activation screen identified transgenic lines that can induce wing grooming [61]. However, many of them have broad expression. It is unclear which specific group of neurons is important for wing grooming. First, I will use the *trans*-Tango method to investigate the morphology of secondary interneurons that receive input from wing mechanosensory neurons. Second, I will search for these interneurons in Fly Bowl dataset [61] wing grooming category to identify transgenic lines that target these neurons. The split Gal4 method [34] will also be used to narrow down the expression pattern.

4.2 Results

4.2.1 Wing grooming can be induced by wing campaniform sensilla in both intact and decapitated flies

Wing campaniform sensilla is associated with an oval shape cuticular dome. It is innervated by a single mechanosensory neuron that responds to cuticle deformations [35]. Wing campaniform sensilla can be classified as proximal or distal sensilla according to their location on the wings. Proximal sensilla project to both brain and ventral nerve cord (VNC). Distal sensilla only project to VNC. Backfilling of a single proximal sensillum shows that its axons branch into three tracts: one ends in SEZ, one ends in VNC around wing neuropil, and the last ends in the metathoracic segment of VNC [62].

I identified *Wing Haltere CS-spGAL4* which labels campaniform sensilla on both wings and haltere. For wing campaniform sensilla, this line consistently labels approximately 20 proximal sensilla (Figure 12B-D). The expression in one or two distal sensilla is observed in some flies. *Wing Haltere CS-spGAL4* induced strong wing grooming upon optogenetic activation (Figure 12F). The same response was not observed when activating haltere campaniform sensilla alone (Figure 4K), which suggests wing campaniform sensilla play the most essential role. The initiation of wing grooming was also observed in decapitated flies (Figure 12F). Therefore, the neural circuits within VNC alone are sufficient for wing grooming. I will focus on the VNC interneurons in this study.

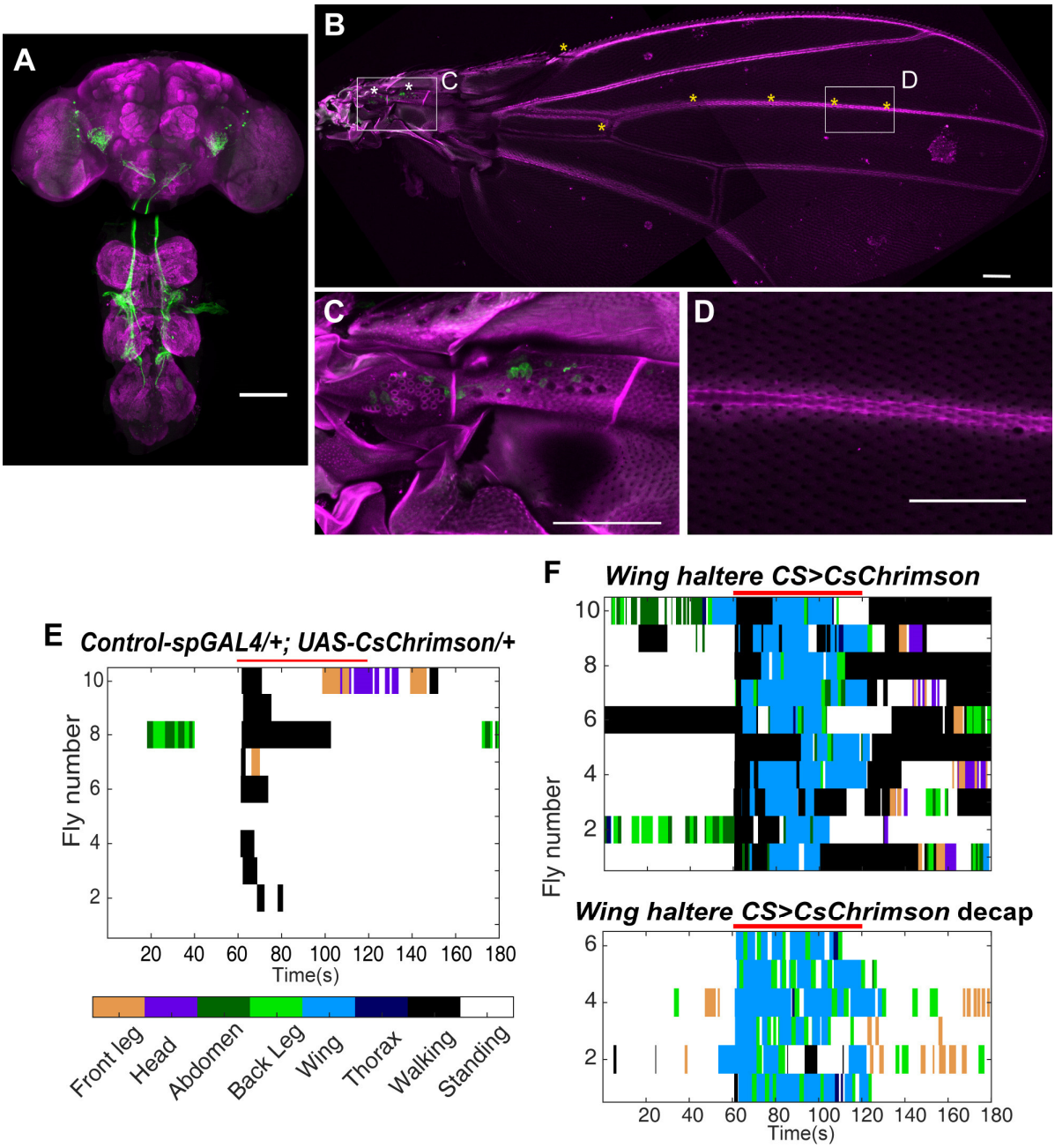

Figure 12. Wing grooming can be induced by activating wing campaniform sensilla in both intact and decapitated flies

(**A-D**) Expression pattern of *Wing haltere CS-spGAL4* in central nervous system (**A**) and wing (**B-D**). Green: anti-GFP. Magenta: anti-Bruchpilot in CNS, cuticle autofluorescence in wing. Proximal campaniform sensilla are indicated by white asterisks, distal campaniform sensilla are indicated by yellow asterisks in **B**. Scale bars, 100μm. (**E**) Ethograms showing grooming behaviors with red light-illumination of control flies. Optogenetic stimulation was given between 60 and 120s, indicated by red line. (**F**) Grooming response induced by optogenetic stimulation of campaniform sensilla in intact (top) and decapitated flies (below).

4.2.2 Anatomical characterization of wing campaniform sensilla post-synaptic neurons

Next, I used the *trans*-Tango method to determine the anatomy of secondary interneurons of wing campaniform sensilla. *trans*-Tango contains two components: axon-localized ligand hGCG::hICAM1::dNRXN1 and receptor-transcription factor chimeric hGCGR::TEVcs::QF [60]. In the experiment, hGCGR::TEVcs::QF is expressed pan-neuronally and hGCG::hICAM1::dNRXN1 is expressed only in campaniform sensilla. In the secondary interneurons, hGCGR::TEVcs::QF receptors are activated trans-synaptically, QF is released to initiate the expression of reporter mtdTomato-3xHA (Figure 13A).

Expression of the *trans*-Tango ligand in wing and haltere campaniform sensilla drives strong signals in both brain and VNC (Figure 13B). Approximately 40 neurons are labeled in the brain, and most of them have cell bodies surrounding SEZ (Figure 13C). In VNC, positive neurons can be found in all three segments (Figure 13D). Axons from haltere campaniform sensilla enter CNS through VNC metathoracic segment (T3) I focus on the first two segments (T1, prothoracic segment; T2, mesothoracic segment) of VNC to identify interneurons specific for wing campaniform sensilla. Approximately 25 tango-positive neurons are located in T1, many of them are ascending neurons which transfer information to the brain. Most neurons are located between the T1 and T2, surrounding wing neuropil region. Approximately 15 neurons are found in T2. Using the anatomy of the tango-positive neurons as a template search image, I selected transgenic lines that target these candidate neurons from Fly Bowl dataset [61] according to position and anatomy.

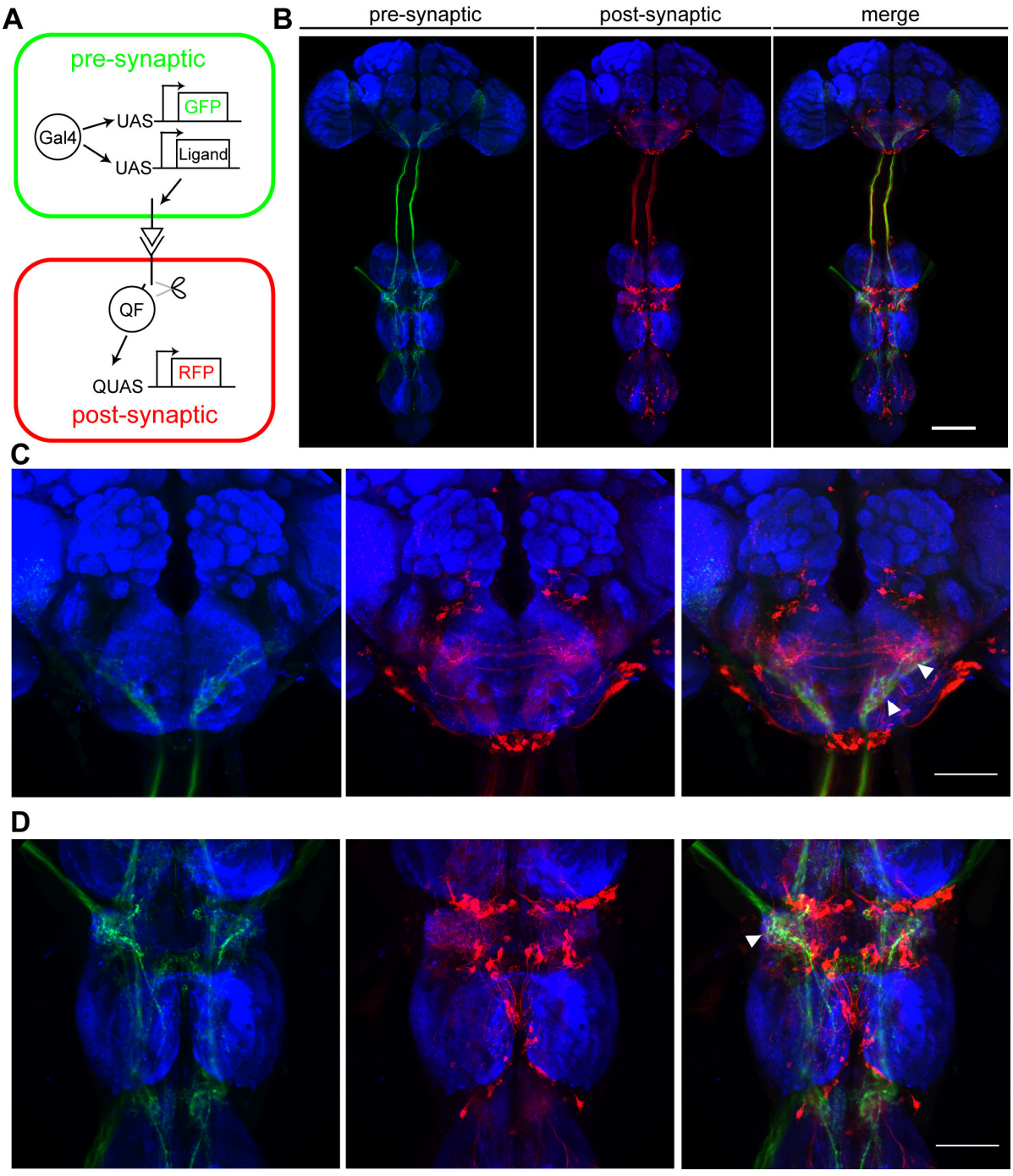

Figure 13. Anatomical characterization of neurons post-synaptic to wing campaniform sensilla
(**A**) Schematic design of *trans*-Tango [60] which is used for anterograde tracing. (**B**) Expression of *trans*-Tango in wing and haltere campaniform sensilla reveals candidate post-synaptic neurons. Green: anti-GFP. Red: anti-HA. Blue: anti-Bruchpilot. Scale bars, 100μm. (**C**, **D**) Higher magnification images of neurons in subesophageal zone (SEZ, **C**) and ventral nerve cord around wing neuropil (**D**). Triangles indicate potential synapses.

4.2.3 R42D02 interneurons in ventral nerve cord receive direct inputs from wing campaniform sensilla and induce wing grooming ipsilaterally

Several interneurons can be found in T2 posterior region from the *trans*-Tango experiment (Figure 13D). Neurons with similar morphology and position are labeled by *R42D02-Gal4* and *R42D02-lexA* transgenic lines. *R42D02-lexA* only labels a pair of neurons in VNC, which I name R42D02 interneurons (Figure 14A). *R42D02-Gal4* labels R42D02 interneurons and ~15 other interneurons in VNC. *R42D02-Gal4* and *R42D02-lexA* also label some fat body, especially in the abdomen (data not shown).

The morphology of R42D02 interneurons suggests they may receive inputs from wing campaniform sensilla and send information to T3. The GRASP method [63] was used to examine the structural connection: one fragment of GFP was expressed using *wing haltere CS-spGAL4*, and the complementary fragment of GFP was expressed using *R42D02-lexA*. Strong reconstituted GFP signals were observed along wing neuropil in experiment flies but not in controls (Figure 14B), which demonstrates that R42D02 interneurons directly contact wing campaniform sensilla.

Activation of R42D02 interneurons with CsChrimson induced strong wing grooming (Figure 14C, D). The same response was also observed in decapitated flies (data not shown). Flies usually clean one wing and then switch to the other. Interestingly, different fly has different preference for wing choice, although neurons on both sides are labeled (Figure 14H). Genetically identical individuals display variability in their behaviors. Individual flies exhibit constant bias in turning direction in Y-maze, which wing is placed on top at rest [64] and the ability of line following during walking [65]. Several factors may contribute to this preference for wing

choice during grooming, such as unequal expression levels of CsChrimson, the asymmetry projection pattern of left and right R42D02, or downstream neurons.

To investigate how the specific side of wing grooming is induced, I performed stochastic activation of R42D02 interneuron on one side. FRT>-dSTOP-FRT>-CsChrimson is expressed using *R42D02-Gal4*. At the same time, R57C10 promoter drives the expression of Flp2::PEST in all neurons. PEST sequence reduces the half-life of Flp2 recombinase [66]. Therefore, in subsets of neurons labeled by *R42D02-Gal4*, Flp2 recombinase removes the stop cassette before CsChrimson and induces its expression. R57C10 promoter also limits the expression of CsChrimson to neurons. Therefore, the non-neural expression of *R42D02-Gal4* does not account for the behavior we observe here. Each individual fly was tested in behavior experiments and then dissected for CNS imaging. R42D02 interneurons receive sensory input from one side and project axons to the other side of body (Figure 14E), but the wing grooming was mainly induced on the same side as the sensory input (Figure 14F, H). Therefore, R42D02 interneurons receive direct inputs from wing campaniform sensilla, project contralaterally but induce wing grooming ipsilaterally.

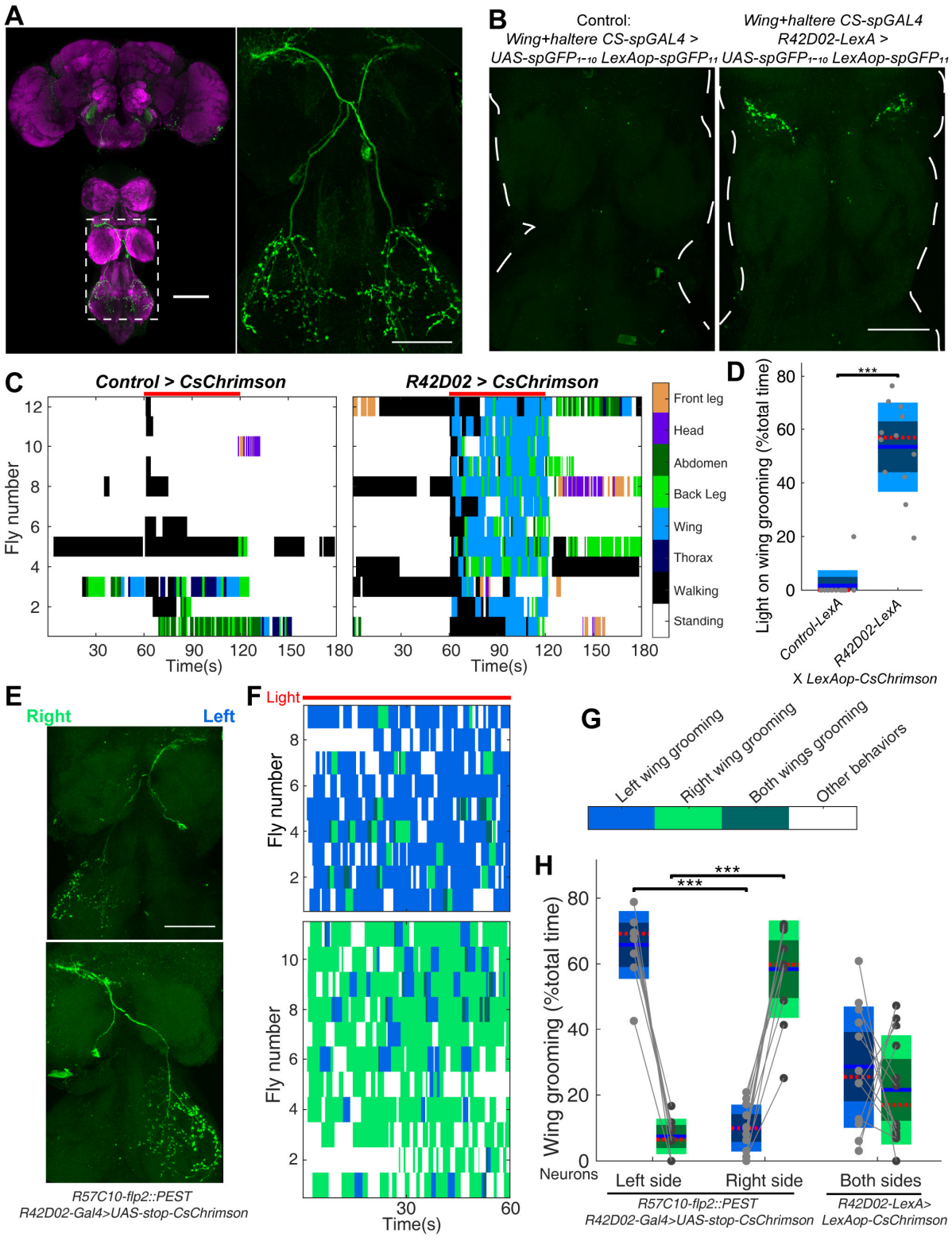

Figure 14. R42D02 interneurons in ventral nerve cord receive direct inputs from wing campaniform sensilla and have contralateral projections but induce wing grooming ipsilaterally

(**A**) Expression pattern of CsChrimson-mVenus (green) driven by *R42D02-LexA* in CNS. Green: anti-GFP. Magenta: anti-Bruchpilot. Scale bars, 100μm. (**B**) GRASP reconstituted GFP signal (green, endogenous fluorescence) between wing campaniform sensilla neurons and R42D02 interneurons in the wing neuropil (right). GRASP signal was not observed in control flies (left). (**C**) Ethograms showing grooming behaviors with red light-illumination of control (left) and *R42D02 > CsChrimson* (right) flies. Optogenetic stimulation was given between 60 and 120s. (**D**) The percent of time that control or *R42D02 > CsChrimson* flies perform wing grooming within 1-minute light activation. The mean is shown as a blue line, 95% confidence intervals for the mean are showed as dark shades. The median is shown as a dotted red line. 1 standard deviation is shown as light color shade. (**E**) Stochastically labelled single R42D02 interneuron on the left (top) or the right side (below). The left-right axis is reversed because of the sample direction. Scale bars, 100μm. (**F**) Different types of wing grooming induced by a single R42D02 interneuron on the left (top) or the right side (below). (**G**) The color code used in the data visualization in **F** and **H**. (**H**) Quantification of different wing grooming behaviors induced by one side or both sides of R42D02 interneurons.

4.3 Discussion

Interneurons with contralateral projections are found in both invertebrates and vertebrates [8,52,65,67–71]. In *Drosophila*, they have been identified in auditory [67], visual [65] and mechanosensory [8] neural circuits. Contralateral projections help animals compare sensory input between left and right [52]. Excitatory contralateral interneurons are also found in larva and contribute to symmetric bilateral muscle contraction [68].

R42D02 interneurons may contribute to left-right legs coordination during wing grooming. Files usually clean one wing at a time. They mainly use the ipsilateral hindleg to clean wing surface. The contralateral hindleg is also lifted from the ground to keep balance. Sometimes, flies coordinate two hindlegs to scratch both surfaces of a single wing. Activation of R42D02 interneurons induce wing grooming in undusted flies, which indicates they may be excitatory interneurons. Therefore, they modulate leg motor neurons on the contralateral side for coordination. At the same time, some downstream neurons of R42D02 interneurons project across the

midline and induce wing grooming ipsilaterally. The alternative hypothesis is that R42D02 interneurons are inhibitory and inhibit wing grooming towards the opposite side.

Therefore, identifying neurotransmitter and downstream neurons are the essential next steps to narrow down the function of R42D02 interneurons. Acetylcholine, GABA and glutamate are the three main neurotransmitters in *Drosophila* CNS. A neuron usually only uses one of the three neurotransmitters [72]. Acetylcholine and glutamate are mainly excitatory, GABA is usually inhibitory. Immunostaining will be used to check the neurotransmitter of R42D02 interneurons. Double labelling between neurotransmitter GAL4 lines [73] and *R42D02-LexA* driver line will also be used to confirm our result.

This project provides an example about how to use various tools to identify the components of a neural circuit. By applying similar methods, we will further investigate other circuit components downstream of R42D02 interneurons. The *trans*-Tango method can be combined with MARCM to reveal the morphology of single downstream neuron [60]. We will investigate whether there are post-synaptic leg motor neurons, as well as interneurons whose projections cross the midline.

5. Discussion, Perspective, and Future Plans

Various innate sequential behaviors have been described in vertebrates [18,19], but the underlying neural circuitry is still largely unknown. Interestingly, 10–15% of all observed self-grooming behaviors in rodents consist of highly stereotyped patterns of sequential movements [20]. This sequence contains four phases: paw

and nose grooming, unilateral face grooming, bilateral head grooming and body licking. Brain lesion studies show that brainstem is crucial for self-grooming initiation while striatum is essential for sequence completion [74,75]. The striatum is also the key region for sequence execution of other behaviors [76], but the exact neurons and circuits are remain to be discovered.

In the first study described here, we investigated how mechanosensory inputs drive sequential grooming in *Drosophila*. We found that the anterior-to-posterior grooming sequence is generated by a simple sensory processing mechanism: flies compare sensory inputs across the body and groom the body part that has the highest sensory input. This spatial comparison could be computed by (unidentified) interneurons which integrate sensory information from different body parts. Therefore, similar to courtship [21], it is possible that a few interneurons can be the key for sequence generation in *Drosophila* grooming.

With a tractable nervous system and a rich behavioral repertoire, *Drosophila* has been a good model organism for neural circuit analysis. Great efforts have been made to develop circuit mapping tools, which can be divided into two categories: anatomical tools and functional tools.

The anatomy of a neural circuit can be reconstructed by either light or electron microscopy. Dense reconstruction from EM images provides an unbiased census for all the neurons and synapses. But its exhaustive nature also brings new challenges for data analysis. Even at the scale of adult *Drosophila*, there are ~135,000 neurons in the brain and ~20,000 neurons in the VNC [77]. Reconstruction of approximately 25,000 neurons in the brain identified approximately 20 million chemical synapses between them [78]. Therefore,

functional analysis is necessary to identify the synapses that are important for a specific behavior. Anatomical tools based on light microscopy are also very useful, especially in regions where the dense construction is still lacking. GRASP and its derivatives X-RASP or t-GRASP can assess neural connectivity between candidate neuron pairs [63,79,80]. Genetically encoded anterograde and retrograde tracing tools are also established in flies. *trans*-Tango and TRACT allow labeling of postsynaptic neurons through ligand-induced transcription factors release [60,81]. BAcTrace encodes a modified Clostridium botulinum neurotoxin A1 (BoNT/A), which can jump retrogradely to activate a transcription factor in presynaptic neurons [82].

More than 12,500 driver lines and various effectors allow us to manipulate neural activity in free-moving flies [77]. However, many driver lines label large groups of neurons, and it can be time consuming to narrow down which group of neurons is actually essential for a specific behavior. Functional tools are also important for confirming synapses identified by EM or GRASP. Presynaptic neurons can be activated by electrode, CsChrimson or ATP-gated cation channel P2X2 [83]; meanwhile, neural activity can be monitored through electrophysiology recording or calcium imaging in potential downstream neurons. Calcium imaging from population of neurons in behaving flies allows us to identify neurons that are highly active during certain behavior [84,85]. But it is still challenging to find a specific driver line to manipulate the target neurons.

In the second project described here, we used both anatomical and functional tools to investigate the neural circuit for wing grooming. The *trans*-Tango method was used to characterize the anatomy of secondary interneurons of wing

campaniform sensilla. This information guided us to select driver lines identified in behavior screen. More tools will be helpful for bridging anatomical and functional information. For example, dataset of neuron morphology alignment between EM and fluorescence microscope will make it easier to identify driver lines for neurons in EM images or vice versa. Trans-synaptic tools such as *trans*-Tango can be modified to not only express fluorescence protein, but also neuron effectors.

With the help of evolving tools, we hope to identify neurons that perform spatial comparisons of sensory inputs and drive behavior choice in the future. One hypothesis is that different grooming behaviors are controlled by separate neural circuits. Mutual inhibition between them determines the behavior choice under different sensory inputs. In larvae, reciprocal inhibition promotes behavior choice between hunch and bend during escape [86]. In adult flies, sensory comparison between left and right legs is processed by the second-order neuron which receives inhibition from the opposite side across the midline [8]. Alternatively, the same group of decision-making neurons are active under different sensory inputs, but the distinct activity patterns determine the corresponding behavior output. In this case, reciprocal inhibition is not necessary [88]. It is also possible that these two mechanisms function at different levels of grooming control: anterior and posterior grooming motifs are performed by different pairs of legs, the choice of them can be controlled by separate neural circuits. Grooming subroutines within each motif are performed by the same pair of legs, where shared decision-making neurons are possible.

Both anatomical and functional methods can be used to test these hypotheses. Using sensory driver lines identified in this work with *trans*-Tango and GRASP, we

can map out the neural circuit that processes anterior or posterior sensory inputs and find the interaction points between them. We can also perform activation or inhibition screen of interneurons in dusted flies. Neurons that promote one grooming behavior but inhibit another will be the candidates involved in competitive interactions. To look for the potential inhibition between anterior and posterior grooming behaviors, we can activate anterior sensory neurons and monitor the decrease of neural activities in VNC using semi-intact preparation. The neural mechanisms for sensory signals comparison and behavior choice remain open questions in neuroscience. My studies provide guidance and genetic tools to investigate it.

6. Materials and Methods

Fly husbandry

Flies *Drosophila melanogaster* were reared on common cornmeal food in 25℃ incubators on a 12 hr light/dark cycle. For optogenetic experiments, larvae were raised on normal food. After eclosion, 1-day old adults were transferred into food containing 0.4 mM all-trans-retinal and reared in the dark for another two days. For olfactory organs amputation, antennae and maxillary palps of 3-day *Canton S* males were removed by fine tweezers. They were given three days to recover before dusting experiments. Eye bristle and compound eye mutants were backcrossed with *Canton S* for five generations before grooming experiments. A full list of fly lines can be found in Appendix.

Identification of fly lines that target sensory neurons

I performed literature research to identify transgenic lines that target different groups of sensory neurons. To identify additional driver lines, I performed a visual screen on CNS expression patterns in the Flylight database [33]. Candidate driver lines were crossed with GFP effector line, GFP expression in sensory neurons was confirmed by peripheral nervous system (PNS) imaging. Split Gal4 approach [34] was used to further refine the expression to sensory neurons.

Immunofluorescence and confocal imaging

For CNS immunostaining, whole flies immobilized with insect pin on abdomen were fixed in 4% PFA for 2 hours on nutator at room temperature. After three 1 min wash in PBT, flies were dissected in PBS buffer to get the whole CNS. CNS samples were further washed by three times in 1 min PBT and then blocked for 30 min in 4% NGS. Staining with primary antibody was performed in 4℃ overnight on a nutator. Samples were then washed 3 times for 20 min in PBT. Secondary antibody incubation was performed for 2 hours in room temperature. Samples were washed again in PBT for 3 times; mounted in VectaShield for imaging. PNS dissection and eye bristles immunostaining was performed using the published protocol [29]. In short, whole flies were washed in 100% ethanol and then PBS, specific body parts were then pulled and mounted in VectaShield on microscope slides for imaging. The following primary antibodies were used: rabbit polyclonal to GFP (Invitrogen A-11122, 1:1000), chicken polyclonal to GFP (Abcam 13970, 1:1000), rabbit anti-HA (Cell Signaling Technologies C29F4, 1:300) and mouse monoclonal brp antibody (DSHB nc82, 1:200). All secondary antibodies were diluted at 1:500. Their category numbers can be found in Appendix. Confocal images were taken on a Zeiss LSM710 microscope. Images were then processed in ImageJ.

In *trans*-Tango and GRASP experiments, flies were raised at 25℃ for 8-10 days before dissection. Endogenous GFP signal was imaged in GRASP experiments.

Morphology of eye bristle mutants

Eye photos of male flies were taken through an SZX 12 Olympus stereomicroscope at different Z positions. Z-series for each fly were registered through BUnwarpJ (https://imagej.net/BUnwarpJ) and converted into single image through Extended Depth of Field plugin (http://bigwww.epfl.ch/demo/edf/).

Recording and analysis of dust-induced grooming

Three chambers were used in fly dusting assay: dusting chamber (24 well corning tissue culture plate #3524), transfer chamber and recording chamber. Dust-induced grooming assays were performed in 21-23℃. 4-7 days male flies were anesthetized on ice and transferred to the middle four wells of transfer chamber. 10-day old males were used in Kir inhibition experiments to increase the expression level of Kir. Flies were left in transfer chamber for 15 min to recover. Around 5 mg Reactive Yellow 86 dust was added into each of the 4 middle wells of dusting chamber. Before use, dust was baked in a 160℃ oven overnight to remove extra moisture. For fly dusting, transfer chamber was aligned with dusting chamber. Flies were tapped into dusting chamber and shaken for 10 times. After dusting, flies and dust were transferred back into transfer chamber. Transfer chamber was banged against an empty pipette tip box to remove extra dust. Dusted flies were then immediately tapped into recording chamber for video recording. The whole dusting process was performed in a WS-6 downflow hood. As undusted control, flies with the same genotype were shaken in chambers without dust. At least 10 individuals were recorded for each genotype.

30 Hz videos were recorded for 50,000 frames (27.78 min) with a DALSA Falcon2 color 4M camera. A white LED ring right was used for illumination. Infrared backlight was used for grooming experiments in the dark. Videos were processed through ABRS to generate ethograms. Grooming modules were described previously [23].

Optogenetics experiments of free-moving flies

After cold anesthesia, flies were left to recover in recording chamber for at least 20 min. Custom-made LED panels (LXM2-PD01-0050, 625nm) were used for light activation from below. 20 Hz 20% light duty cycle was used in all experiments. LED power was adjusted according to the expression level and behavioral response of different lines. Light intensity was measured by Thorlabs S130VC power sensor coupled with PM100D console. The light intensity used in the experiments are: *Control-spGAL4* (8.4 mW/cm^2), *Bristle-spGAL4-1* (0.84 mW/cm^2), *Bristle-spGAL4-2* (0.84 mW/cm^2), *Wing+haltere CS-spGAL4* (5.6 mW/cm^2), *Control-GAL4* (8.4 mW/cm^2), *CO-GAL4* (1.4 mW/cm^2), *SR-GAL4* (8.4 mW/cm^2), *HP-GAL4* (5.6 mW/cm^2), *MD-GAL4* (5.6 mW/cm^2), *Antennal CO-spGAL4* (5.6 mW/cm^2), *R21D12-GAL4* (8.4 mW/cm^2), *R73D10-GAL4* (5.6 mW/cm^2), *R86D09-GAL4* (5.6 mW/cm^2), *VT028607-GAL4* (8.4 mW/cm^2), *R14F05-GAL4* (8.4 mW/cm^2), *Gr33a-GAL4* (5.6 mW/cm^2), *Gr64f-GAL4* (5.6 mW/cm^2), *Ppk28-GAL4* (5.6 mW/cm^2), *Orco-GAL4* (5.6 mW/cm^2), *Or56a-GAL4* (5.6 mW/cm^2), *R42D02-GAL4* (5.6 mW/cm^2), *Control-LexA* (5.6 mW/cm^2 and 11.2 mW/cm^2), *R42G12-LexA* (5.6 mW/cm^2), *R42D02-LexA* (11.2 mW/cm^2). 30Hz videos were recorded by IDS UI-3370CP-C-HQ camera and manually annotated in VCode or automatically annotated by ABRS (https://github.com/AutomaticBehaviorRecognitionSystem/ABRS).

Fly-on-a-ball experiment

Experimental rig was set up as protocol described previously [84] with modifications. In short, 3 days female was tethered to a size 1 insect pin through UV glue. Air flow was used to support the 10mm diameter foam ball (LAST-A-FOAM FR-7120 material). Air flow (500-600 ml/min) passed through water before foam ball for humidification. Two Doric Lenses fiber LEDs (CLED_635) with custom-made collimator were used to target head and posterior end of abdomen. Thorlabs NE513B neutral density filters were used to adjust light intensity. To determine the light intensity, I first did preliminary experiments to see which light combination give us approximately equal amount of anterior and posterior grooming. Then I used that intensity with changed anterior light intensity or changed posterior light intensity to investigate how sensory input ratio change affects behavior choice. Because it is hard to measure the illumination area, LED light power rather than intensity was used. LED driver was connected with National Instruments USB-6008 DAQ to control light ramp. 20 Hz 20% light duty cycle was used for both anterior and posterior light stimulations in *R74C07>ChrimsonR* flies. Each fly was tested in two different light conditions. The order of light conditions was random. 20 min recovery time was given between different conditions. 30Hz videos were recorded with a Point Grey BFS-U3-13Y3M-C camera and manually annotated in VCode.

Computational model

d(t) stands for dust amount on different body parts. For simulation of *Canton S* flies, *d(t)* was set up according to mechanosensory bristle numbers on different body parts. Initial dust on front legs and back legs was set to be 200. *a(t)* represents neural activities induced by dust. It follows a normal distribution whose mean is *d(t)*,

the relationship between $d(t)$ and $\sigma(t)$ is estimated according to the bristle electrophysiology recordings [7]:

$$a(t) \sim N(d(t), \sigma(t)^2), \sigma(t) = d(t)/5$$

Winner-take-all layer determines the body part which has the highest neural activity ($a_{body\ part}(t)$) as the winner. The winner body part will be groomed in this grooming iteration. If the winner is leg, some percent of dust ($10dr$) will be discarded. Otherwise, some percent of dust (dr) will be transformed from winner body part to the corresponding legs:

$$d_{front/back\ legs}(t+1) = d_{front/back\ legs}(t) - d_{front/back\ legs}(t) * 10dr \text{ (winner is leg)}$$

$$d_{winner}(t+1) = d_{winner}(t) - d_{winner}(t) * dr,\ d_{front/back\ legs}(t+1) = d_{front/back\ legs}(t) + d_{winner}(t) * dr$$

(winner is other body parts)

We did not model the grooming bout duration. It was drawn from duration distributions of different grooming modules we got from two manually labeled dusted *Canton S* ethograms.

Quantification and Statistical Analysis

Data analysis was performed in MATLAB 2016b and 2017b. Wilcoxon signed-rank test was used for two related samples. Wilcoxon rank-sum test was used for two independent samples. Kruskal-Wallis test with Wilcoxon rank-sum post hoc were used for three or more independent samples.

Data was plotted with notBoxPlot (https://github.com/raacampbell/notBoxPlot) function. Each dot is one fly. The mean is shown as a blue line, 95% confidence intervals for the mean are showed as dark shades. The median is shown as a dotted red line. 1 standard deviation is shown as light color shade.

shadedErrorBar (https://github.com/raacampbell/shadedErrorBar) function was used for grooming progression figures. For dusting experiments or model simulations. Behavior probabilities were calculated every 16 seconds in a sliding 32-second time window. For optogenetic experiments with 5s and 1min light activation, behavior probabilities were calculated every 2.5 seconds in a sliding 5-second time window. For optogenetic experiments with 5min and 14min light activation, behavior probabilities were calculated every 5 seconds in a sliding 10-second time window. Each data point is the average among all individuals. The shade stands for the standard error of mean.

To quantify the ratio of anterior grooming to posterior grooming in each time window, we first calculated the duration (as frame number) fly performed anterior or posterior grooming for that interval. If the fly did not perform any grooming behavior during that period. That time point for the fly was discarded from further analysis. Otherwise, the log ratio of anterior grooming to posterior grooming was calculated as following:

$$\text{Log}_{10}(\text{Anterior grooming/Posterior grooming}) = \text{Log}_{10}\{[\text{Frame number (anterior grooming)} +1]/ [\text{Frame number (posterior grooming)} +1]\}$$

To calculate the anterior grooming half-time, we first calculated the duration of total anterior grooming within 5 min assay time. The anterior grooming half-time is the time point when flies finish half of the total anterior grooming. When flies start from similar anterior grooming starting point, the faster grooming progression is, the earlier flies finish half of total anterior grooming.

References

1. Zhang, N., Guo, L., and Simpson, J.H. (2020). Spatial Comparisons of Mechanosensory Information Govern the Grooming Sequence in Drosophila. Curr. Biol. *30*, 988-1001.e4.
2. Ramdya, P., Lichocki, P., Cruchet, S., Frisch, L., Tse, W., Floreano, D., and Benton, R. (2015). Mechanosensory interactions drive collective behaviour in Drosophila. Nature *519*, 233–236.
3. Li, J., Zhang, W., Guo, Z., Wu, S., Jan, L.Y., and Jan, Y.-N. (2016). A Defensive Kicking Behavior in Response to Mechanical Stimuli Mediated by Drosophila Wing Margin Bristles. J. Neurosci. *36*, 11275–11282.
4. Tuthill, J.C., and Wilson, R.I. (2016). Mechanosensation and Adaptive Motor Control in Insects. Curr. Biol. *26*, R1022–R1038.
5. Tsubouchi, A., Yano, T., Yokoyama, T.K., Murtin, C., Otsuna, H., and Ito, K. (2017). Topological and modality-specific representation of somatosensory information in the fly brain. Science (80-.). *358*, 615–623. Available at: http://www.sciencemag.org/lookup/doi/10.1126/science.aan4428.
6. Kernan, M.J. (2007). Mechanotransduction and auditory transduction in Drosophila. Pflügers Arch. J. Physiol. *454*, 703–720.
7. Walker, R.G., Willingham, A.T., and Zuker, C.S. (2000). A Drosophila mechanosensory transduction channel. Science *287*, 2229–2234.
8. Tuthill, J.C., and Wilson, R.I. (2016). Parallel Transformation of Tactile Signals in Central Circuits of Drosophila. Cell *164*, 1046–1059.
9. Yorozu, S., Wong, A., Fischer, B.J., Dankert, H., Kernan, M.J., Kamikouchi,

A., Ito, K., and Anderson, D.J. (2009). Distinct sensory representations of wind and near-field sound in the Drosophila brain. Nature *458*, 201–205.

10. Kamikouchi, A., Inagaki, H.K., Effertz, T., Hendrich, O., Fiala, A., Gopfert, M.C., and Ito, K. (2009). The neural basis of Drosophila gravity-sensing and hearing. Nature *458*, 165–171.
11. Mamiya, A., Gurung, P., and Tuthill, J.C. (2018). Neural Coding of Leg Proprioception in Drosophila. Neuron *100*, 636-650.e6.
12. Dickerson, B.H., de Souza, A.M., Huda, A., and Dickinson, M.H. (2019). Flies regulate wing motion via active control of a dual-function gyroscope. Curr. Biol. *29*, 3517–3524.
13. Maniates-Selvin, J.T., Hildebrand, D.G.C., Graham, B.J., Kuan, A.T., Thomas, L.A., Nguyen, T., Buhmann, J., Azevedo, A.W., Shanny, B.L., and Funke, J. (2020). Reconstruction of motor control circuits in adult Drosophila using automated transmission electron microscopy. bioRxiv.
14. Desai, B.S., Chadha, A., and Cook, B. (2014). The stum gene is essential for mechanical sensing in proprioceptive neurons. Science (80-.). *343*, 1256–1259.
15. Zhang, Y. V, Aikin, T.J., Li, Z., and Montell, C. (2016). The basis of food texture sensation in Drosophila. Neuron *91*, 863–877.
16. Lazopulo, S., Lazopulo, A., Baker, J.D., and Syed, S. (2019). Daytime colour preference in Drosophila depends on the circadian clock and TRP channels. Nature *574*, 108–111.
17. Benjamin, S.P., and Zschokke, S. (2004). Homology, behaviour and spider webs: web construction behaviour of Linyphia hortensis and L. triangularis

(Araneae: Linyphiidae) and its evolutionary significance. J. Evol. Biol. *17*, 120–130.

18. Hall, Z.J., Meddle, S.L., and Healy, S.D. (2015). From neurons to nests: nest-building behaviour as a model in behavioural and comparative neuroscience. J. Ornithol. *156*, 133–143.
19. Van Iersel, J.J.A., and Tinbergen, N. (1948). " Displacement Reactions" in the Three-Spined Stickleback. Behaviour *1*, 56–63.
20. Kalueff, A. V, Stewart, A.M., Song, C., Berridge, K.C., Graybiel, A.M., and Fentress, J.C. (2016). Neurobiology of rodent self-grooming and its value for translational neuroscience. Nat. Rev. Neurosci. *17*, 45.
21. McKellar, C.E., Lillvis, J.L., Bath, D.E., Fitzgerald, J.E., Cannon, J.G., Simpson, J.H., and Dickson, B.J. (2019). Threshold-Based Ordering of Sequential Actions during Drosophila Courtship. Curr. Biol. *29*, 426-434.e6.
22. Qiao, B., Li, C., Allen, V.W., Shirasu-Hiza, M., and Syed, S. (2018). Automated analysis of long-term grooming behavior in Drosophila using a k-nearest neighbors classifier. Elife *7*.
23. Seeds, A.M., Ravbar, P., Chung, P., Hampel, S., Midgley, F.M., Mensh, B.D., and Simpson, J.H. (2014). A suppression hierarchy among competing motor programs drives sequential grooming in Drosophila. Elife *3*, e02951.
24. Glaze, C.M., and Troyer, T.W. (2006). Temporal structure in zebra finch song: implications for motor coding. J. Neurosci. *26*, 991–1005.
25. Mackevicius, E.L., and Fee, M.S. (2018). Building a state space for song learning. Curr. Opin. Neurobiol. *49*, 59–68.
26. Geddes, C.E., Li, H., and Jin, X. (2018). Optogenetic Editing Reveals the

Hierarchical Organization of Learned Action Sequences. Cell *174*, 32-43.e15.

27. Ravbar, P., Branson, K., and Simpson, J.H. (2019). An automatic behavior recognition system classifies animal behaviors using movements and their temporal context. J. Neurosci. Methods *326*, 108352.

28. Szebenyi, A.L. (1969). Cleaning behaviour in Drosophila melanogaster. Anim. Behav. *17*, 641–651.

29. Hampel, S., McKellar, C.E., Simpson, J.H., and Seeds, A.M. (2017). Simultaneous activation of parallel sensory pathways promotes a grooming sequence in drosophila. Elife *6*.

30. Yanagawa, A., Guigue, A.M.A., and Marion-Poll, F. (2014). Hygienic grooming is induced by contact chemicals in Drosophila melanogaster. Front. Behav. Neurosci. *8*. Available at: http://journal.frontiersin.org/article/10.3389/fnbeh.2014.00254/abstract.

31. Vandervorst, P., and Ghysen, A. (1980). Genetic control of sensory connections in drosophila. Nature *286*, 65–67.

32. Corfas, G., and Dudai, Y. (1989). Habituation and dishabituation of a cleaning reflex in normal and mutant Drosophila. J. Neurosci. *9*, 56–62.

33. Jenett, A., Rubin, G.M., Ngo, T.-T.B., Shepherd, D., Murphy, C., Dionne, H., Pfeiffer, B.D., Cavallaro, A., Hall, D., Jeter, J., *et al.* (2012). A GAL4-driver line resource for Drosophila neurobiology. Cell Rep. *2*, 991–1001.

34. Pfeiffer, B.D., Ngo, T.-T.B., Hibbard, K.L., Murphy, C., Jenett, A., Truman, J.W., and Rubin, G.M. (2010). Refinement of tools for targeted gene expression in Drosophila. Genetics *186*, 735–755.

35. Dickinson, M.H., and Palka, J. (1987). Physiological properties, time of

development, and central projection are correlated in the wing mechanoreceptors of Drosophila. J. Neurosci. *7*, 4201–4208.

36. Hampel, S., Franconville, R., Simpson, J.H., and Seeds, A.M. (2015). A neural command circuit for grooming movement control. Elife *4*.

37. Klapoetke, N.C., Murata, Y., Kim, S.S., Pulver, S.R., Birdsey-Benson, A., Cho, Y.K., Morimoto, T.K., Chuong, A.S., Carpenter, E.J., Tian, Z., *et al.* (2014). Independent optical excitation of distinct neural populations. Nat. Methods *11*, 338–346.

38. Cadigan, K.M., and Nusse, R. (1996). wingless signaling in the Drosophila eye and embryonic epidermis. Development *122*, 2801–12. Available at: http://www.ncbi.nlm.nih.gov/pubmed/8787754.

39. Baines, R.A., Uhler, J.P., Thompson, A., Sweeney, S.T., and Bate, M. (2001). Altered electrical properties in Drosophila neurons developing without synaptic transmission. J. Neurosci. *21*, 1523–1531.

40. Sweeney, S.T., Broadie, K., Keane, J., Niemann, H., and O'Kane, C.J. (1995). Targeted expression of tetanus toxin light chain in Drosophila specifically eliminates synaptic transmission and causes behavioral defects. Neuron *14*, 341–351.

41. Hodge, J.J.L. (2009). Ion channels to inactivate neurons in Drosophila. Front. Mol. Neurosci. *2*, 13.

42. Pezier, A., Jezzini, S.H., Marie, B., and Blagburn, J.M. (2014). Engrailed alters the specificity of synaptic connections of Drosophila auditory neurons with the giant fiber. J. Neurosci. *34*, 11691–11704.

43. Thum, A.S., Knapek, S., Rister, J., Dierichs-Schmitt, E., Heisenberg, M., and

Tanimoto, H. (2006). Differential potencies of effector genes in adult Drosophila. J. Comp. Neurol. *498*, 194–203.

44. Montell, C. (2009). A taste of the Drosophila gustatory receptors. Curr. Opin. Neurobiol. *19*, 345–353.

45. Stensmyr, M.C., Dweck, H.K.M., Farhan, A., Ibba, I., Strutz, A., Mukunda, L., Linz, J., Grabe, V., Steck, K., Lavista-Llanos, S., *et al.* (2012). A conserved dedicated olfactory circuit for detecting harmful microbes in drosophila. Cell *151*, 1345–1357.

46. Böröczky, K., Wada-Katsumata, A., Batchelor, D., Zhukovskaya, M., and Schal, C. (2013). Insects groom their antennae to enhance olfactory acuity. Proc. Natl. Acad. Sci. *110*, 3615–3620. Available at: http://www.pnas.org/lookup/doi/10.1073/pnas.1212466110.

47. Montell, C. (2012). Drosophila visual transduction. Trends Neurosci. *35*, 356–363.

48. Cadigan, K.M., Jou, A.D., and Nusse, R. (2002). Wingless blocks bristle formation and morphogenetic furrow progression in the eye through repression of Daughterless. Development *129*, 3393–3402.

49. Roseland, C.R., and Schneiderman, H.A. (1979). Regulation and metamorphosis of the abdominal histoblasts of Drosophila melanogaster. Wilhelm Roux's Arch. Dev. Biol. *186*, 235–265.

50. Hartenstein, V., and Posakony, J.W. (1989). Development of adult sensilla on the wing and notum of Drosophila melanogaster. Development *107*, 389–405.

51. Gaudry, Q., Hong, E.J., Kain, J., de Bivort, B.L., and Wilson, R.I. (2013). Asymmetric neurotransmitter release enables rapid odour lateralization in

Drosophila. Nature *493*, 424–428.

52. Suver, M.P., Matheson, A.M.M., Sarkar, S., Damiata, M., Schoppik, D., and Nagel, K.I. (2019). Encoding of Wind Direction by Central Neurons in Drosophila. Neuron *102*, 828-842.e7.

53. Liu, M., Sharma, A.K., Shaevitz, J.W., and Leifer, A.M. (2018). Temporal processing and context dependency in Caenorhabditis elegans response to mechanosensation. Elife *7*.

54. Pierce-Shimomura, J.T., Morse, T.M., and Lockery, S.R. (1999). The fundamental role of pirouettes in Caenorhabditis elegans chemotaxis. J. Neurosci. *19*, 9557–9569.

55. Luo, J., Shen, W.L., and Montell, C. (2017). TRPA1 mediates sensation of the rate of temperature change in Drosophila larvae. Nat. Neurosci. *20*, 34–41.

56. Vogelstein, J.T., Park, Y., Ohyama, T., Kerr, R.A., Truman, J.W., Priebe, C.E., and Zlatic, M. (2014). Discovery of brainwide neural-behavioral maps via multiscale unsupervised structure learning. Science (80-.). *344*, 386–392.

57. Takemura, S., Bharioke, A., Lu, Z., Nern, A., Vitaladevuni, S., Rivlin, P.K., Katz, W.T., Olbris, D.J., Plaza, S.M., and Winston, P. (2013). A visual motion detection circuit suggested by Drosophila connectomics. Nature *500*, 175–181.

58. Zheng, Z., Lauritzen, J.S., Perlman, E., Robinson, C.G., Nichols, M., Milkie, D., Torrens, O., Price, J., Fisher, C.B., and Sharifi, N. (2018). A complete electron microscopy volume of the brain of adult Drosophila melanogaster. Cell *174*, 730–743.

59. Lo, L., and Anderson, D.J. (2011). A Cre-dependent, anterograde

transsynaptic viral tracer for mapping output pathways of genetically marked neurons. Neuron *72*, 938–950.

60. Talay, M., Richman, E.B., Snell, N.J., Hartmann, G.G., Fisher, J.D., Sorkaç, A., Santoyo, J.F., Chou-Freed, C., Nair, N., and Johnson, M. (2017). Transsynaptic mapping of second-order taste neurons in flies by trans-Tango. Neuron *96*, 783–795.

61. Robie, A.A., Hirokawa, J., Edwards, A.W., Umayam, L.A., Lee, A., Phillips, M.L., Card, G.M., Korff, W., Rubin, G.M., and Simpson, J.H. (2017). Mapping the neural substrates of behavior. Cell *170*, 393–406.

62. Ghysen, A. (1980). The projection of sensory neurons in the central nervous system of Drosophila: choice of the appropriate pathway. Dev. Biol. *78*, 521–541.

63. Feinberg, E.H., VanHoven, M.K., Bendesky, A., Wang, G., Fetter, R.D., Shen, K., and Bargmann, C.I. (2008). GFP Reconstitution Across Synaptic Partners (GRASP) defines cell contacts and synapses in living nervous systems. Neuron *57*, 353–363.

64. Buchanan, S.M., Kain, J.S., and De Bivort, B.L. (2015). Neuronal control of locomotor handedness in Drosophila. Proc. Natl. Acad. Sci. *112*, 6700–6705.

65. Linneweber, G.A., Andriatsilavo, M., Dutta, S.B., Bengochea, M., Hellbruegge, L., Liu, G., Ejsmont, R.K., Straw, A.D., Wernet, M., and Hiesinger, P.R. (2020). A neurodevelopmental origin of behavioral individuality in the Drosophila visual system. Science (80-.). *367*, 1112–1119.

66. Li, X., Zhao, X., Fang, Y., Jiang, X., Duong, T., Fan, C., Huang, C.-C., and Kain, S.R. (1998). Generation of destabilized green fluorescent protein as a

transcription reporter. J. Biol. Chem. *273*, 34970–34975.

67. Lai, J.S.-Y., Lo, S.-J., Dickson, B.J., and Chiang, A.-S. (2012). Auditory circuit in the Drosophila brain. Proc. Natl. Acad. Sci. *109*, 2607–2612.

68. Heckscher, E.S., Zarin, A.A., Faumont, S., Clark, M.Q., Manning, L., Fushiki, A., Schneider-Mizell, C.M., Fetter, R.D., Truman, J.W., and Zwart, M.F. (2015). Even-skipped+ interneurons are core components of a sensorimotor circuit that maintains left-right symmetric muscle contraction amplitude. Neuron *88*, 314–329.

69. Gebhardt, M., and Honegger, H.-W. (2001). Physiological characterisation of antennal mechanosensory descending interneurons in an insect (Gryllus bimaculatus, Gryllus campestris) brain. J. Exp. Biol. *204*, 2265–2275.

70. Knebel, D., Worner, J., Rillich, J., Nadler, L., Ayali, A., and Couzin-Fuchs, E. (2018). The subesophageal ganglion modulates locust inter-leg sensory-motor interactions via contralateral pathways. J. Insect Physiol. *107*, 116–124.

71. Suster, M.L., Kania, A., Liao, M., Asakawa, K., Charron, F., Kawakami, K., and Drapeau, P. (2009). A novel conserved evx1 enhancer links spinal interneuron morphology and cis-regulation from fish to mammals. Dev. Biol. *325*, 422–433.

72. Lacin, H., Chen, H.-M., Long, X., Singer, R.H., Lee, T., and Truman, J.W. (2019). Neurotransmitter identity is acquired in a lineage-restricted manner in the Drosophila CNS. Elife *8*, e43701.

73. Simpson, J.H. (2016). Rationally subdividing the fly nervous system with versatile expression reagents. J. Neurogenet. *30*, 185–194.

74. Berridge, K.C. (1989). Progressive degradation of serial grooming chains by descending decerebration. Behav. Brain Res. *33*, 241–253.

75. Cromwell, H.C., and Berridge, K.C. (1996). Implementation of action sequences by a neostriatal site: a lesion mapping study of grooming syntax. J. Neurosci. *16*, 3444–3458.

76. Bailey, K.R., and Mair, R.G. (2006). The role of striatum in initiation and execution of learned action sequences in rats. J. Neurosci. *26*, 1016–1025.

77. Bates, A.S., Janssens, J., Jefferis, G.S.X.E., and Aerts, S. (2019). Neuronal cell types in the fly: single-cell anatomy meets single-cell genomics. Curr. Opin. Neurobiol. *56*, 125–134.

78. Xu, C.S., Januszewski, M., Lu, Z., Takemura, S., Hayworth, K., Huang, G., Shinomiya, K., Maitin-Shepard, J., Ackerman, D., and Berg, S. (2020). A connectome of the adult drosophila central brain. BioRxiv.

79. Macpherson, L.J., Zaharieva, E.E., Kearney, P.J., Alpert, M.H., Lin, T.-Y., Turan, Z., Lee, C.-H., and Gallio, M. (2015). Dynamic labelling of neural connections in multiple colours by trans-synaptic fluorescence complementation. Nat. Commun. *6*, 1–9.

80. Shearin, H.K., Quinn, C.D., Mackin, R.D., Macdonald, I.S., and Stowers, R.S. (2018). t-GRASP, a targeted GRASP for assessing neuronal connectivity. J. Neurosci. Methods *306*, 94–102.

81. Huang, T., Niesman, P., Arasu, D., Lee, D., De La Cruz, A.L., Callejas, A., Hong, E.J., and Lois, C. (2017). Tracing neuronal circuits in transgenic animals by transneuronal control of transcription (TRACT). Elife *6*, e32027.

82. Cachero, S., Gkantia, M., Bates, A.S., Frechter, S., Blackie, L., McCarthy, A.,

Sutcliffe, B., Strano, A., Aso, Y., and Jefferis, G.S.X.E. (2020). BAcTrace a new tool for retrograde tracing of neuronal circuits. bioRxiv.

83. Yao, Z., Macara, A.M., Lelito, K.R., Minosyan, T.Y., and Shafer, O.T. (2012). Analysis of functional neuronal connectivity in the Drosophila brain. J. Neurophysiol. *108*, 684–696.

84. Chen, C.-L., Hermans, L., Viswanathan, M.C., Fortun, D., Aymanns, F., Unser, M., Cammarato, A., Dickinson, M.H., and Ramdya, P. (2018). Imaging neural activity in the ventral nerve cord of behaving adult Drosophila. Nat. Commun. *9*, 4390.

85. Seelig, J.D., Chiappe, M.E., Lott, G.K., Dutta, A., Osborne, J.E., Reiser, M.B., and Jayaraman, V. (2010). Two-photon calcium imaging from head-fixed Drosophila during optomotor walking behavior. Nat. Methods *7*, 535–540.

86. Jovanic, T., Schneider-Mizell, C.M., Shao, M., Masson, J.-B., Denisov, G., Fetter, R.D., Mensh, B.D., Truman, J.W., Cardona, A., and Zlatic, M. (2016). Competitive Disinhibition Mediates Behavioral Choice and Sequences in Drosophila. Cell *167*, 858-870.e19.

87. Cameron, P., Hiroi, M., Ngai, J., and Scott, K. (2010). The molecular basis for water taste in Drosophila. Nature *465*, 91–95.

88. Kristan, W.B. (2008). Neuronal decision-making circuits. Curr. Biol. *18*, R928-32.

89. Shirangi, T.R., Wong, A.M., Truman, J.W., and Stern, D.L. (2016). Doublesex regulates the connectivity of a neural circuit controlling Drosophila male courtship song. Dev. Cell *37*, 533–544.

90. von Reyn, C.R., Breads, P., Peek, M.Y., Zheng, G.Z., Williamson, W.R., Yee,

A.L., Leonardo, A., and Card, G.M. (2014). A spike-timing mechanism for action selection. Nat. Neurosci. *17*, 962–970.

91. Nern, A., Pfeiffer, B.D., and Rubin, G.M. (2015). Optimized tools for multicolor stochastic labeling reveal diverse stereotyped cell arrangements in the fly visual system. Proc. Natl. Acad. Sci. *112*, E2967–E2976.

Appendix

Table 1. Reagent or resource used in the study

REAGENT or RESOURCE	SOURCE	IDENTIFIER
Antibodies		
chicken polyclonal to GFP	Abcam	Cat#13970
rabbit polyclonal to GFP	Invitrogen	Cat#A-11122
rabbit monoclonal anti-HA	Cell Signaling Technologies	Cat# C29F4
mouse monoclonal brp antibody	DSHB	Cat#AB_2314866
anti-chicken Alexa Fluor 488	Invitrogen	Cat#A-11039
anti-rabbit Alexa Fluor 488	Invitrogen	Cat#A-11008
anti-rabbit Alexa Fluor 568	Invitrogen	Cat# A-11011
anti-mouse Alexa Fluor 633	Invitrogen	Cat#A-21052
Chemicals, Peptides, and Recombinant Proteins		
Reactive Yellow 86	Organic Dyestuffs Corporation	CAS 61951-86-8
Insect-a-slip	BioQuip Products	Cat#2871A
UV glue	Bondic	N/A
Experimental Models: Organisms/Strains		
Canton S	Bloomington Stock Center	RRID: BDSC_64349
Control-spGAL4: BPp65ADZp (attP40); BPZpGDBD (attP2)	Bloomington Stock Center	RRID: BDSC_79603
Bristle-spGAL4-1: R38B08-AD; R81E10-DBD	Bloomington Stock Center	RRID: BDSC_71032 ; RRID: BDSC_68529
Bristle-spGAL4-2: R38B08-AD; R70C11-DBD	Bloomington Stock Center	RRID: BDSC_71032 ; RRID: BDSC_70292

Wing+haltere CS-spGAL4: R83H05-AD; R31H10-DBD	Bloomington Stock Center	RRID: BDSC_68688 ; RRID: BDSC_69835
Control-GAL4: pBDPGal4U	Bloomington Stock Center	RRID: BDSC_68384
CO-GAL4: iav-GAL4	Bloomington Stock Center	RRID: BDSC_52273
SR-GAL4: stum-GAL4	Bloomington Stock Center	RRID: BDSC_58777
HP-GAL4: R48A07-GAL4	Bloomington Stock Center	RRID: BDSC_50340
MD-GAL4: ppk-GAL4	Bloomington Stock Center	RRID: BDSC_32079
Eye bristle-spGAL4: R38B08-AD; VT043775-DBD	Bloomington Stock Center	RRID: BDSC_71032 ; RRID: BDSC_73728
Antennal CO-spGAL4: R61D08-AD; R27H08-DBD	Bloomington Stock Center	RRID: BDSC_71105 ; RRID: BDSC_69106
R74C07-GAL4	Bloomington Stock Center	RRID: BDSC_39847
R52A06-GAL4	Bloomington Stock Center	RRID: BDSC_38810
R21D12-GAL4	Bloomington Stock Center	RRID: BDSC_48946
R73D10-GAL4	Bloomington Stock Center	RRID: BDSC_39819
R86D09-GAL4	Bloomington Stock Center	RRID: BDSC_40459
VT028607-GAL4	Vienna Drosophila Resource Center	Cat#203789
R14F05-GAL4	Bloomington Stock Center	RRID: BDSC_49257
Gr33a-GAL4	Bloomington Stock Center	RRID: BDSC_31425

Gr64f-GAL4	Bloomington Stock Center	RRID: BDSC_57669
ppk28-GAL4	[87]	N/A
Or56a-GAL4	Bloomington Stock Center	RRID: BDSC_23896
Orco-GAL4	Bloomington Stock Center	RRID: BDSC_23292
R42D02-GAL4	Bloomington Stock Center	RRID: BDSC_41250
Control-LexA: pBDPLexAp65U (attP40)	Bloomington Stock Center	RRID: BDSC_77691
R42G12-LexA	Bloomington Stock Center	RRID: BDSC_53643
R42D02- LexA	Bloomington Stock Center	RRID: BDSC_54264
20XUAS-CsChrimson-mVenus (attp18)	Bloomington Stock Center	RRID: BDSC_55134
20XUAS-ChrimsonR-mCherry (attp18)	[37]	N/A
20XUAS-FRT>STOP>FRT-CsChrimson-mVenus (attP2)	[89]	N/A
13XLexAop2-CsChrimson-mVenus (attp18)	Bloomington Stock Center	RRID: BDSC_55137
10XUAS-IVS-eGFPKir2.1 (attP2)	[90]	N/A
10XUAS-IVS-mCD8::GFP (attP2)	Bloomington Stock Center	RRID: BDSC_32185
UAS-myrGFP.QUAS-mtdTomato-3xHA (su(Hw)attP8); trans-Tango (attP40)	Bloomington Stock Center	RRID: BDSC_77124
R57C10-FLP2::PEST	[91]	N/A
P[sev-wg, w⁻]	[38]	N/A
eya^{2}	Bloomington Stock Center	RRID: BDSC_2285
so^{D}	Bloomington Stock Center	RRID: BDSC_4287

orco[1]	Bloomington Stock Center	RRID: BDSC_23129
orco[2]	Bloomington Stock Center	RRID: BDSC_23130
Software and Algorithms		
Adobe Illustrator	https://www.adobe.com/products/illustrator.html	RRID:SCR_010279
MATLAB	http://www.mathworks.com/products/matlab/	RRID:SCR_001622
Python	http://www.python.org/	RRID:SCR_008394
Fiji	http://fiji.sc/	RRID:SCR_002285
VCode	http://social.cs.uiuc.edu/projects/vcode.html	N/A
Automatic Behavior Recognition System (ABRS)	[27]	N/A